NTNU – Trondheim
Norwegian University of
Science and Technology

Pipeline Walking of High Pressure/Temperature Flowlines

Camilla Tveråmo

Marine Technology
Submission date: June 2013
Supervisor: Svein Sævik, IMT
Co-supervisor: Pål Foss, IKM

Norwegian University of Science and Technology
Department of Marine Technology

NTNU Trondheim
Norges teknisk-naturvitenskapelige universitet
Institutt for marin teknikk

MASTER THESIS SPRING 2013

for

Stud. tech. Camilla Tveråmo

Pipeline Walking of high pressure/temperature flowlines

Kryp av brønnstrømsrør ved høye trykk og temperaturer

Short high pressure/temperature flowlines are exposed to frequent start-up and shut-downs during the design life. One of the phenomena related to this behaviour is that the flowline starts to move ("walk") towards the cool end, thus being detrimental for the end connection design. The aim of the present thesis is to get a clear understanding of the physical processes governing pipeline walking phenomena. The thesis work is to be carried out as follows:

1. Literature study, Offshore pipeline technology in general including design loads, failuremodes and design criteria, pipeline-soil interaction, heat transfer including steady state and transient behaviour, pipeline expansion and walking including a review of the SAFEBUCK JIP.
2. Give a proper description of the walking phenomenon.
3. In cooperation with the co-advisor define a relevant walking scenario that include all relevant physical quantities, i.e. to define a flowline design scenario where walking phenomena will occur.
4. Modelling and simulation, i.e. to model the flowline design scenario in SIMLA. In cooperation with the co-advisor define a relevant sensitivity matrix for varying relevant parameters and perform simulations.
5. Analytical modelling and simulation, i.e. based on the understanding obtained from the simulation, create an analytical model and compare the results with the simulation.
6. Conclusions and recommendations for further work

The thesis work assumes that all necessary input data are provided by IKM.

The work scope may prove to be larger than initially anticipated. Subject to approval from the supervisors, topics may be deleted from the list above or reduced in extent.

In the thesis the candidate shall present his personal contribution to the resolution of problems within the scope of the thesis work

Theories and conclusions should be based on mathematical derivations and/or logic reasoning identifying the various steps in the deduction.

The candidate should utilise the existing possibilities for obtaining relevant literature.

Thesis format

The thesis should be organised in a rational manner to give a clear exposition of results, assessments, and conclusions. The text should be brief and to the point, with a clear language. Telegraphic language should be avoided.

The thesis shall contain the following elements: A text defining the scope, preface, list of contents, summary, main body of thesis, conclusions with recommendations for further work, list of symbols and acronyms, references and (optional) appendices. All figures, tables and equations shall be numerated.

The supervisors may require that the candidate, in an early stage of the work, presents a written plan for the completion of the work.

The original contribution of the candidate and material taken from other sources shall be clearly defined. Work from other sources shall be properly referenced using an acknowledged referencing system.

The report shall be submitted in two copies:
- Signed by the candidate
- The text defining the scope included
- In bound volume(s)
- Drawings and/or computer prints which cannot be bound should be organised in a separate folder.

Ownership
NTNU has according to the present rules the ownership of the thesis. Any use of the thesis has to be approved by NTNU (or external partner when this applies). The department has the right to use the thesis as if the work was carried out by a NTNU employee, if nothing else has been agreed in advance.

Thesis supervisors:

Prof. Svein Sævik, NTNU
Pål Foss, IKM

Deadline: June 10, 2013

Trondheim, January, 2013

Svein Sævik

Candidate – date and signature:

Preface

This master thesis have been written in the spring of 2013 as the final part of a MSc degree in Marine Technology at The Norwegian University of Science and Technology.

The interest for pipeline technology was triggered in the late fall of 2012 when I was offered a position at IKM Ocean Design in Trondheim. I wanted my thesis to focus on a topic relevant for my future job, and in cooperation with my supervisor Pål Foss, I decided to write my master thesis on the subject of pipeline walking.

In the presented work an introduction to offshore pipeline technology in general, and pipeline walking in particular, is given. In addition a share of the literature in the field is presented, with focus on the SAFEBUCK JIP. The theory acquired through this process have been utilised through a case study, where several factors that influence the behaviour of walking have been assessed.

I would like to thank my supervisor at NTNU, Prof. Svein Sævik, for good guidance and academic support throughout the course of working with this thesis. I would also like to thank my supervisor at IKM Ocean Design, Pål Foss, for insight into the pipeline industry, as well as the necessary input data.

Trondheim, June 10th 2013

Camilla Tveråmo

Abstract

The offshore pipeline industry are facing more complex design challenges as the oil and gas industry moves into deeper water in search for hydrocarbons. One of these challenges are related to high pressure/high temperature pipelines subjected to frequent start-up and shut-downs during its' lifetime. One consequence of this kind of load cycles is that the pipeline may move cycle wise and axially towards its' cold end, which may be detrimental for the end connection design. This phenomenon is termed pipeline walking.

The SAFEBUCK Joint Industry Project was initiated in 2002 to assess the challenges connected to pipeline walking, in addition to other related issues. Through this project several aspects affecting the walking behaviour have been established. These factors have, in this thesis, been addressed through a sensitivity analysis, where the seabed conditions – hereby the equivalent friction factor – the seabed slope, the effect of a global lateral buckle and the effect of a connected SCR have been included.

The sensitivity study was performed on a pipeline modelled in SIMLA with 900 beam elements, each connected with a spring to a seabed beam element. This original case have here been labelled the base case. Four cases were analysed, were one factor were changed throughout each of the cases. The pipeline was subjected to a transient temperature profile in each case, provided by IKM Ocean Design, to simulate the heat transfer in a pipeline.

For the seabed conditions case, the walk per load cycle increased with increasing equivalent friction factor up to a certain point, before the walk per load cycle decreased as the equivalent friction factor continued to increase. The seabed slope case showed that the relationship between walk per cycle and increasing angle is approximately linear. In addition it was established that when the seabed slope is steep enough, the pipeline will walk towards its' warm end. In the global lateral buckle case on could observe that the effective axial friction force was relieved in the buckle, and that the walk per cycle increased as the length of the buckle increased. When a steel catenary riser tension was introduced, the axial movement of the pipeline appeared to fluctuate around the walk per cycle values for the base case.

An analytical analysis was performed, however, the accordance between the numerical and analytical results was not as good as predicted. For this reason an improvement of the analytical model is suggested for further work. An other topic which is relevant for further work is an extension of the seabed conditions case to include mobilisation length. Additional sub-cases in the steel catenary riser case, as well as creating a new case by combining the impact from several walking inducing factors are other possible topics.

Sammendrag

Rørledningsindustrien møter stadig komplekse utfordringer etter hvert som olje- og gassindustrien opererer på stadig dypere vann i søken etter fossilt brennstoff. En av utfordringene er relatert til høyt trykk/høy temperatur-rørledninger, som er utsatt for jevnlige oppstarter og nedstengninger i løpet av sin levetid. Én konsekvens av å bli utsatt for denne typen lastsykluser, er at rørledningen vil bevege seg syklisk og aksielt mot sin kalde ende. Dette fenomenet kalles *pipeline walking*, eller *kryp av brønnstrømsrør*. Den aksielle bevegelsen, og påfølgende permanente forflytningen, kan være ødeleggende for endekoblingen til rørledningen.

I 2002 ble industriprosjektet SAFEBUCK initiert for å studere utfordringene knyttet til kryp, i tillegg til andre relaterte problemstillinger. Gjennom dette prosjektet har flere aspekter, som sammen påvirker kryp av brønnstrømsrør, blitt etablert. Disse faktorene har i denne masteroppgaven blitt studert gjennom en sensitivitetsanalyse, hvor sjøbunnsegenskapene – her representert ved den ekvivalente aksielle friksjonsfaktoren – sjøbunnshelningen, effekten av en global, lateral krumning av røret, og effekten av å koble et stigerør til den kalde enden av røret har blitt inkludert.

Sensitivitetsstudien ble utført på en rørledning modellert i SIMLA. Modellen består av 900 bjelkeelementer, som hver og en er koblet med fjær til et sjøbunnselement. Fire tilfeller ble analysert, hvor én faktor ble forandret for hvert av tilfellene. En tidsvarierende temperaturprofil ble brukt for å modellere varmeoverføringen i rørledningen. Denne profilen ble gitt som input av IKM Ocean Design, og ble brukt for at temperaturforandringene skulle være så autentiske som mulig.

For sjøbunnsforholdtilfellet kunne man se at kryp per lastsyklus økte med økende ekvivalent friksjonsfaktor, opp til et gitt punkt. Etter dette minket kryp per lastsyklus, mens den ekvivalente friksjonsfaktoren fortsatte å øke. Sjøbunnshelningstilfellet viste at forholdet mellom kryp per syklus og sjøbunnsvinkelen er omtrent lineær. I tillegg kom det fram at når sjøbunnshelningen blir bratt nok, vil rørledningen krype mot sin varme ende. I tilfellet med en global, lateral krumning ble det observert at den effektive friksjonskraften ble avlastet i krumningen, og at kryp per syklus økte i takt med lengden på kurven. Når et stigerør ble introdusert, viste det seg at aksialbevegelsen fluktuerte rundt den jevne bevegelsen som ble

observert for den originale casen. Den originale casen ble kun utsatt for varierende temperatur, og fungerte dermed som sammenlikningsgrunnlag for de andre fire tilfellene her beskrevet.

De numeriske resultatene fra SIMLA ble sammenliknet med resultater fra en analytisk modell. Det viste seg at de analytiske og de numeriske resultatene ikke samsvarte så godt som forventet. Av denne grunn er en forbedring av den analytiske modellen et mulig utgangspunkt for videre arbeid. Et annet tema som er relevant for videre arbeid er en utvidelse av sjøbunnsegenskaptilfellet, slik at dette inkluderer mobiliseringslengde. I tillegg kan flere undertilfeller for stigerørtilfellet legges til, slik at en større forståelse for denne faktoren kan bli oppnådd. Avslutningsvis kan nye tilfeller skapes ved å kombinere de overnevnte tilfellene, for å se hvilken innvirkning disse kombinasjonene vil ha på fenomenet kryp av brønnstrømsrør.

Contents

List of Figures

List of Tables

List of Symbols and Acronyms

FEM	Finite Element Method
FPS	Floating Production System
ID	Internal Diameter
JIP	Joint Industry Project
KP	Kilometre Post
OD	Outer Diameter
SCR	Steel Catenary Riser
$SMTS$	Specified Minimum Tensile Strength
$SMYS$	Specified Minimum Yield Stress
$IKM\ OD$	IKM Ocean Design
A_i	Cross-Sectional Area of Pipe Inside Diameter [m^2]
D	Outside Diameter of a Pipeline [m]
E	Young's Modulus [N/m^2]
H	Original Water Depth [m]
H_{new}	New Water Depth [m]
L	Pipeline Length [m]
$L_{seafloor}$	Sea Floor Length [m]
S_R	SCR Tension [N]
W	Submerged Weight of the Pipeline [N/m]
X_{ab}	Length Between Virtual Anchor Points [m]

ΔP	The Change in Fully Constrained Force [N]
Δ_R	Walk per Cycle Caused by SCR [m]
Δ_α	Walk per Cycle Caused by Seabed Slope [m]
α	Seabed Angle [deg]
ϵ	Axial Strain [-]
γ	Mobilisation Length [mm]
κ	Coefficient of Thermal Expansion [1/°C]
μ_a	Equivalent Axial Friction Factor [-]
ν	Poisson's Ratio [-]
ω	Frequency of the FPS
ϕ	Phase Displacement
ρ	Density of Seawater [kg/m^3]
θ	Operating Temperature [1/°C]
f	Effective Axial Friction Force in a Pipeline [N/m]
f^*	Friction Force at which Cyclic Constraint Occurs [N/m]
p_e	External Pressure [Pa]
p_i	Internal Pressure [Pa]
t	Wall Thickness of a Pipeline [m]

Chapter 1

Introduction

In the oil and gas industry pipeline technology have been in constant development since its' humble beginnings in California a century ago [Guo et al., 2005]. Today, as the offshore pipeline industry moves into more complex conditions, it faces several challenges. One of these challenges are related to high temperature/high pressure pipelines, which are situated on the seabed, and subjected to frequent start-ups and shut-downs during its' life cycle. One of the phenomena connected to this situation is that the pipeline moves axially towards its' cold end, which is the end of the pipeline furthest from the well. This global, axial displacement of the pipeline is termed *pipeline walking*.

The aim of this thesis is to give an introduction to the offshore pipeline industry, with focus on the topics related to the concept of pipeline walking. Further, the phenomena of pipeline walking will be presented and described. To be able to obtain a clear understanding of this phenomena, a walking scenario will be defined. This case study will include relevant physical quantities, so that walking will occur. In the aim of gaining a larger insight into the walking phenomenon, several walking inducing factors will be assessed through the sensitivity analysis, performed with the software SIMLA. These factors' effect on pipeline walking will be documented, and presented. The results from the case study will, in agreement with the supervisor, be compared to analytical solutions already existing in the literature [Sævik, 2013].

The main source of information is articles concerning pipeline walking and related topics. This thesis have been written in cooperation with IKM Ocean Design. The co-supervisor at IKM OD, as well as provided internal reports, have thus been sources of information. The SAFEBUCK Joint Industry Project have contributed to several articles on the subject of pipeline walking, and have been a considerable source when writing this thesis. All references are listed in the Bibliography.

This thesis starts off by introducing the offshore pipeline industry in Chapter 2,

before the walking phenomenon is outlined in Chapter 3. A brief review of the SAFEBUCK JIP will be presented in Chapter 4. The information about the case study and its' results can be found in Chapter 5 and Chapter 6, respectively. Chapter 7 and Chapter 8 concentrate on conclusions and possible further work.

Chapter 2

Offshore Pipeline Technology

The subjects presented in this chapter will generally concern the topic of offshore pipeline technology. It has been chosen to focus on the topics most relevant for pipeline walking, thus the sections may vary when it comes to depth and details outlined.

As earlier mentioned, pipelines have been used in the offshore industry for approximately a century, and are widely in use today. Offshore pipelines can be classified as shown below [Bai and Bai, 2005].

- Export (transportation) pipelines
- Flowlines to transfer product from a platform to export lines
- Water injection or chemical injection flowlines
- Flowlines to transfer product between platforms, subsea manifolds and satellite wells
- Pipeline bundles

An illustration of this classification can be seen in Figure 2.1, which is provided by [Guo et al., 2005].

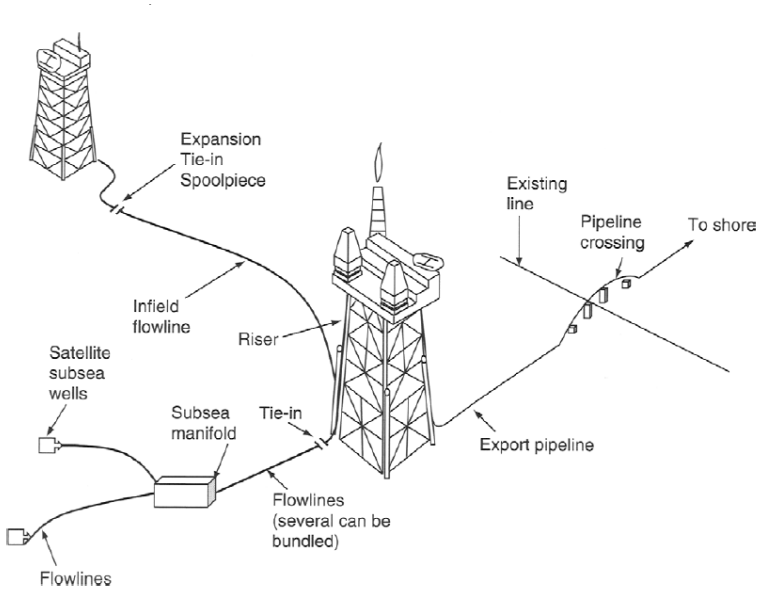

Figure 2.1: The Use of Offshore Pipelines

Figure 2.1 above show the use of pipelines in the offshore industry. This thesis' main focus is pipelines that are susceptible to walking. To be able to understand the walking phenomenon properly, an introduction to pipeline design will be given.

2.1 Pipeline Design

When designing a pipeline there are several factors that need to be taken into account, such as design loads and failure mechanisms. These factors will be briefly introduced in this section.

A subsea pipeline resting on the seabed is susceptible to internal pressure due to the transported medium in the pipeline, external hydrostatic pressure, temperature loads and bending [Jee, 2013]. The internal pressure induce a tensile hoop stress in the pipe wall, which is given in Equation 2.1 below. Assuming a thin wall approximation, the hoop stress σ_h is given by

$$\sigma_h = (p_i - p_e)\frac{D-t}{2t} \tag{2.1}$$

where p_i is the internal pressure, p_e is the external pressure, D is the outside diameter of the pipeline and t is the wall thickness. If this stress reaches the ultimate tensile strength of the material, the pipeline may burst. This is the failure mechanism connected to internal pressure.

If the external pressure become excessive, compressive hoop stress will be induced, and the pipeline may collapse. This is the failure mechanism connected to external pressure.

External pressure can also lead to a local buckle, which often is induced by several combined loadings. These combined loadings may consist of internal or external pressure, bending moment and an axial load due to change in temperature. Local buckling is thus the failure mechanism connected to so-called third party interference.

There are two approaches to pipeline design; allowable stress design and limit-state design. The first approach is the traditional kind, where the basis is to consider the worst case loads together with the minimum possible strength, and in addition apply a safety factor. On the other hand, limit-state design is based on the probability of worst failure mode occurring, in correlation with the consequence of this happening. Both approaches result in an acceptable design in the end [Jee, 2013].

Other phenomena that needs to be taken into account in the design phase are global lateral and upheaval buckling, as well as pipeline walking. Lateral buckling is Euler buckling induced in a pipeline laying on the seabed surface. The lateral buckling of the pipeline relieves axial loading. Upheaval buckling is also Euler buckling, and is relevant for buried pipelines, where the axial force increase due to increasing temperature and pressure. This forces the pipe to displace vertically. Upheaval buckles tend to be more severe than lateral buckles. The reason for this is that the deflection in an upheaval buckle is concentrated in one upheaval, while lateral buckles tend to snake on the seabed [Jee, 2013].

As earlier stated, pipeline walking is the globally axial displacement of a pipeline. The pipeline walks cycle wise towards the cool end in correspondence with the start-ups and shut-downs during the design life. These movements are thus detrimental for the end connection design.

One of the main drivers behind pipeline walking, is the loads induced by heat transfer in the pipeline. For this reason the topic of heat transfer will be introduced next.

2.2 Heat Transfer

When a pipeline is in operating condition, the well medium will heat the pipeline from the inlet end and axially outwards in the pipeline. At the same time there

will be an external heat loss by convection to the surrounding sea water. The temperature decay due to the ambient temperature along the pipeline may be modelled with an exponential profile [Jee, 2013].

Heat transfer may be regarded both as steady state and transient, dependant on which case one is dealing with. As stated above, the temperature will fall as the flow travels along the pipeline due to convection. The arrival temperature, i.e. the temperature at the outlet, of the flow medium may be determined by a steady state analysis. However, if the steady flow condition is interrupted by e.g. maintenance work, the pipeline content will cool down. At this point the heat transfer becomes a transient condition.

The transient heat transfer have properties of thermal conductivity, density and specific heat capacity, while the steady state heat transfer is a property of thermal conductivity alone. The temperature conditions in the case study in this thesis is described by transient heat transfer.

Heat transfer may lead to the pipeline expansion, which is the topic that will be outlined in the next section.

2.3 Pipeline Expansion

Given an exposed pipeline on a flat seabed with free ends, the pipeline will tend to expand when internal temperature and pressure rise to operating conditions. As a result of this pipeline expansion, the frictional resistance of the seabed soil will be mobilised, and an axial compressive force opposing this expansion will thus arise. Consequently, an effective axial compressive force will build up in the pipeline. This effective force increase from the free ends until a force equilibrium is reached.

Whether such a force equilibrium is met, depends on the available friction resistance. If this friction resistance is not sufficient to restrain the pipeline completely at any point along the pipeline, the pipeline in question is a so-called "short" pipeline. In this case, a form of force equilibrium will exist, and this is called a *virtual anchor point*. Given constant friction and pipe properties along the pipeline, this virtual anchor point will be situated at the middle of the pipeline. See Figure 2.2a, gathered from [IKM, 20xx].

If there is sufficient frictional resistance present, the strain that is caused by the frictional resistance will counterbalance the sum of thermal and pressure strains. In other words further movement is prevented, and this pipeline is a so-called "long" pipeline. In this case a section of the pipeline will be fully restrained, and this portion of the pipeline is often referred to as the *anchor zone*, with one anchor point in each end of the zone. See Figure 2.2b, gathered from [IKM, 20xx].

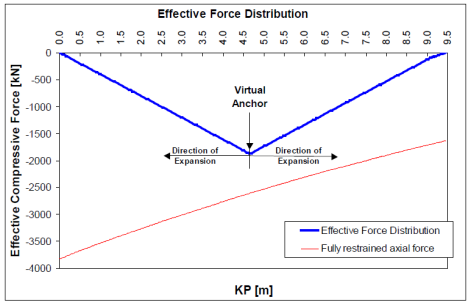

(a) Effective Force Distribution for Short Pipeline

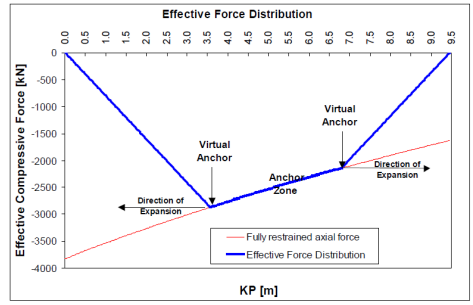

(b) Effective Force Distribution for Long Pipeline

Figure 2.2: Effective Force Distribution for Long and Short Pipelines

The theory behind long and short pipelines will be further outlined in Section 3.1 and Section 3.2 in Chapter 3.

2.4 Pipeline/Soil Interaction

As outlined in Section 2.3 above, an expanding pipeline due to increasing temperature and pressure, will induce an axial compressive force in the pipeline. This behaviour is dependant of the pipeline/soil interaction, which will be further explained in this section.

According to [Bruton et al., 2008] the pipe/soil response is the greatest uncertainty in the design of pipelines prone to walking. Most previous research into pipe/soil interaction has concerned stability under hydrodynamic loading, and not the actual interaction described in the paragraph above. The subject of pipe/soil interaction becomes more and more important as subsea pipelines are required to operate at higher temperatures and pressures. This can lead to uncontrolled lateral buckling, as well as global axial displacement. To be able to assess these two phenomena, and especially the latter, a correct modelling of the pipe/soil properties is essential.

The pipe/soil interaction model consists of a seabed stiffness and an equivalent friction definition to represent the soil resisting any movement of the pipe [Bai and Bai, 2005]. The interaction between pipe and soil is usually modelled by attaching pipe/soil elements in intervals along the pipeline length [Bruton et al., 2008]. These elements represent the axial and lateral forces that influence the pipe/soil interaction.

To be able to model the pipe/soil interaction, a simple friction factor is used, although this may represent an over-simplification of the behaviour in question [Bruton et al., 2008]. A non-linear force/displacement response is thus better to

represent pipe/soil behaviour, and is represented by an equivalent friction factor. This coefficient is given by dividing the maximum resistance in the pipeline by the submerged weight of the pipeline. The equivalent friction for sand is mainly based on coulumb friction, while clay is usually modelled with the use of diagrams including peak friction [Foss, 2013].

Although a friction factor is used to model the pipe/soil interaction, there are several factors that influence this behaviour. These include embedment of the pipeline, the soil conditions in general and the previous history of pipe movement [Bruton et al., 2008]. For this reason it is advisable to include both upper an lower bound values for the equivalent friction factor. This may be explained by Figure 2.3, which is provided by [Bruton et al., 2008].

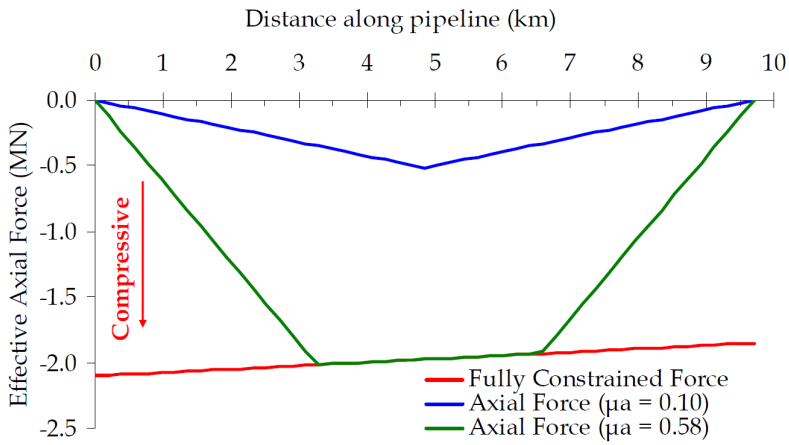

Figure 2.3: Effective Axial Force for two values of Equivalent Friction Factor μ_a

In Figure 2.3 two equivalent friction factors are used, an upper value of $\mu_a = 0.58$ and a lower value of $\mu_a = 0.10$. With reference to Figure 2.2 in Section 2.3 one can see that with $\mu_a = 0.10$ the pipeline behaves like a short pipeline, while with $\mu_a = 0.58$ it behaves like a long pipeline. Thus the pipeline will walk for the lower bound equivalent friction coefficient, and not walk for the upper bound equivalent friction coefficient.

The fully constrained force, represented by a red line in Figure 2.3 above, is the maximum axial force that can occur in a pipeline and is the driving force with respect to axial expansion and structural response [Bruton et al., 2008]. There is a slight fall in the fully constrained force due to heat loss to the environment. The effective axial forces of the pipeline are zero at the free ends, since they are free to expand.

The extent of pipeline walking is highly dependant of the pipe/soil interaction. The

subjects introduced in this section will be further outlined through the explanation of the pipeline walking phenomenon in the following chapter.

Chapter 3

Pipeline Walking

As stated in the introduction and in the previous chapter, pipeline walking is a global, axial displacement of an entire pipeline due changes in operating conditions, and especially due to subsequent start-up and shut-down cycles, i.e. cyclic loading. Over several cycles this can lead to a significant total displacement of the pipeline, and thus be detrimental to the end connection design.

According to [Carr et al., 2008] walking itself is not a limit state, but without consideration it can lead to

- over-stressing spoolpieces/jumpers
- loss of tension in steel catenary risers
- increased loading within a lateral buckle
- need for restraint using anchors
- route-curve pullout of restrained system

The earlier introduced short pipelines are most prone to walking, which occur under cyclic loading. Pipeline walking does not reduce with the number of cycles [Carr et al., 2008]. The factors in the following bullet list influence the walking behaviour. These factors are

- thermal gradients along the pipeline
- the seabed conditions
- the seabed slope
- tension created by a steel catenary riser

In this chapter these factors will be investigated, and the walking phenomenon will be further described and outlined.

3.1 Long and Short Pipelines

In [Tørnes et al., 2000] it is stated that whether a pipeline behaves like a long or short pipeline in operating conditions is the most important question when investigating if a pipeline is prone to walk or not. For this reason the theory of long and short pipelines will be outlined in this section.

Given a pipeline with free ends resting on a flat seabed, where constant pressure and temperature is applied; as earlier described, the pipeline will expand, and an effective axial force will consequently build up in the pipeline due to the mobilised forces in the seabed. The effective axial force builds up from zero at the free ends, and increase towards the middle of the pipeline.

3.1.1 Long Pipelines

For a long pipeline the effective axial force will increase to a point where it will counteract the sum of pressure and thermal strains. At this point the anchor zone, introduced in Section 2.3, arise. The pipeline is now fully constrained, and no axial displacement can occur. This development is illustrated in Figure 3.1, provided by [Tørnes et al., 2000].

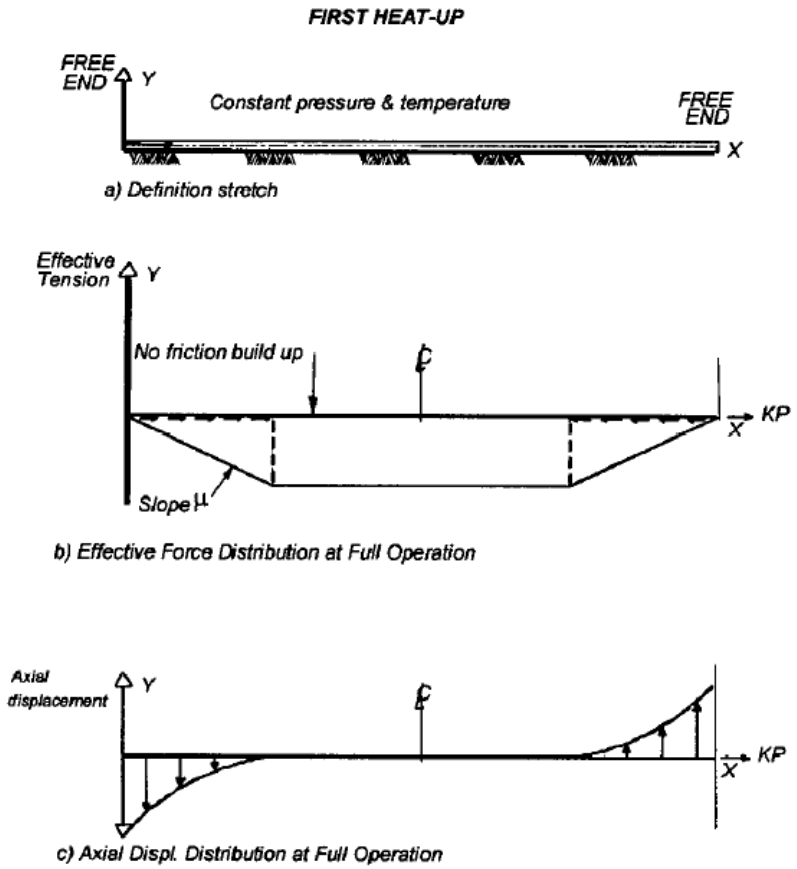

Figure 3.1: Long Pipeline Development

The slope μ in Figure 3.1 b) above is the earlier introduced equivalent axial friction factor. It is given by

$$\mu_a = \frac{f}{W} \tag{3.1}$$

where f is the effective axial friction force [N/m] and W is the submerged unit weight [N/m] [Carr et al., 2008]. It should be noted that the constant anchor zone in Figure 3.1 b) should have had a slope due to heat loss, like shown in Figure 2.3 in Section 2.4. The fully constrained force in Figure 3.1 b) is shown to be constant for simplicity.

3.1.2 Short Pipelines

If the earlier introduced pipeline do not reach the point where the effective axial force counteracts the sum of pressure and thermal strains, the pipeline will be defined as short. The pipeline is thus fully mobilised, and axial displacement along the whole length will occur. In this case a sort of balance will still arise, and this is the virtual anchor point first mentioned in Section 2.3.

The development for a short pipeline is shown in Figure 3.2, also provided by [Tørnes et al., 2000], in the same manner as for the long pipeline.

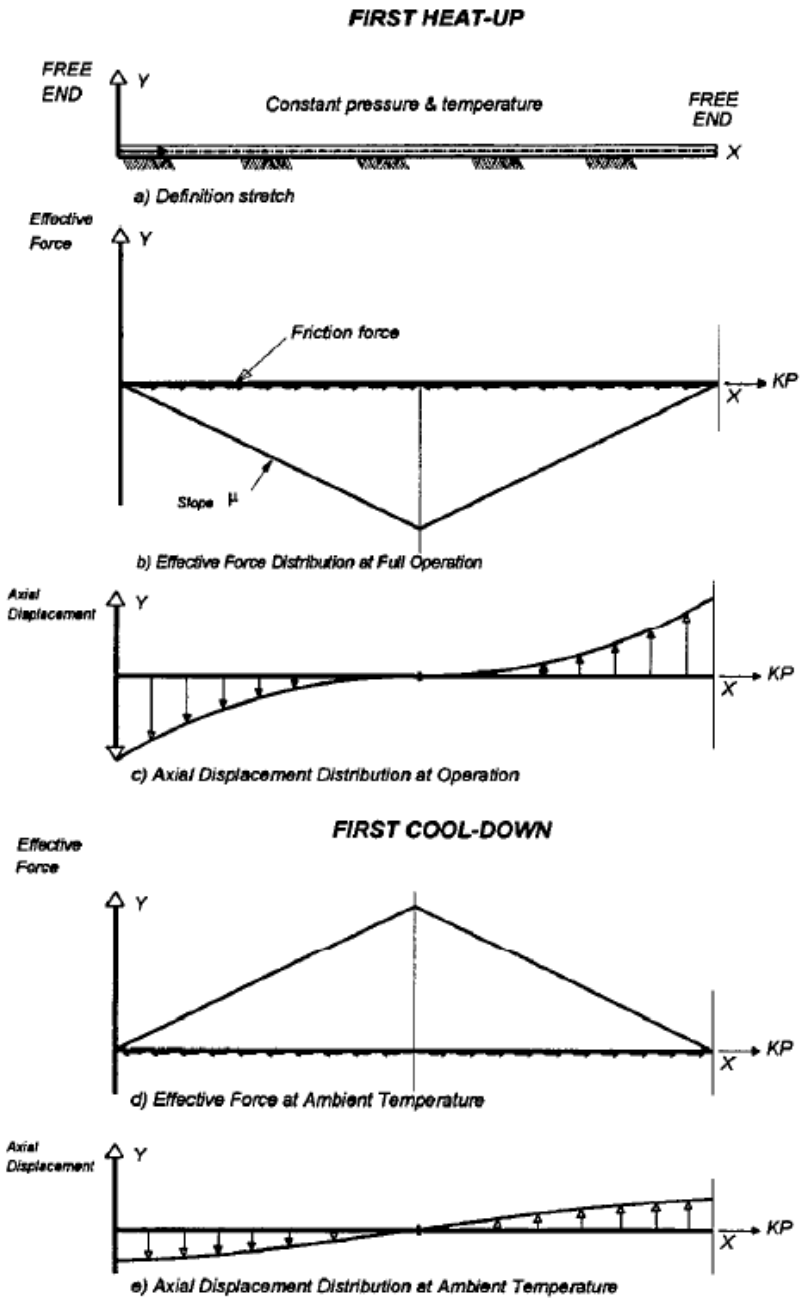

Figure 3.2: Short Pipeline Development

The virtual anchor point is where the effective compressive force has its' peak, and where the stationary point is located [Tørnes et al., 2000]. This becomes clear when studying Figure 3.2 b). Due to symmetry, the virtual anchor point is located at the middle of the pipeline. Examples of cases where the virtual anchor point is not located at the middle, will be given in Section 3.3. But first, the walking mechanisms and relevant definitions will be presented.

3.2 Walking Mechanisms and Definitions

Figure 3.2 in the previous section also show the cool-down of the pipeline. As the temperature and pressure decrease, the pipeline will tend to contract. In this process frictional resistance will develop, and thus oppose the movement. However, the pipeline and seabed must travel a small distance relative to each other before the full frictional resistance has been build up in the opposite direction [Tørnes et al., 2000]. This distance is equal to twice the mobilisation length γ, which can be seen in Figure 3.2 and Figure 3.1 above. The mobilisation length is defined as the amount of axial elastic displacement that occur before the full effective friction force is generated [Carr et al., 2008].

In short this means that the pipeline does not walk back towards its' initial position as soon as the cool-down process start, this is dependant of the mobilisation length. As a consequence, the pipeline will not contract all the way back to this original position. This forth, but not all the way back, process – which leads to a global displacement of the whole pipeline – is the walk in *pipeline walking*.

This displacement is illustrated in Figure 3.3 below.

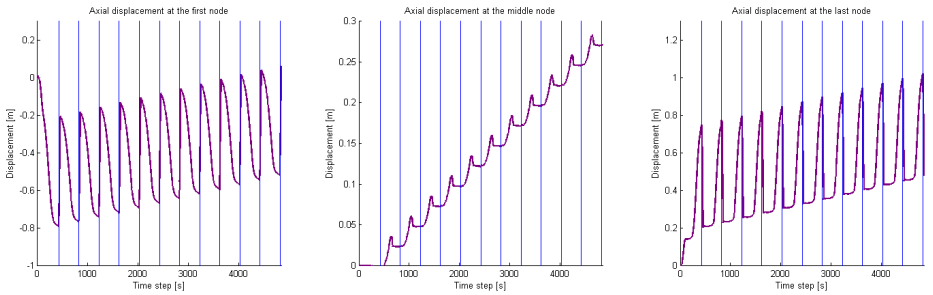

Figure 3.3: Axial Displacement of a Pipeline for the Base Case in the Case Study

Figure 3.3 show the displacement of the (from left to right) first, middle and last node of the pipeline in the base case analysed in this thesis. Details around this case study will be presented in Chapter 5. The blue, vertical lines represent the starting point for each load cycle, that is one heat-up and one cool-down. From the figure,

and particularly by studying the plot of the middle node's movement, one can see the movement described in the paragraph above, and the mechanisms becomes more evident. Figure 3.4 is a more detailed version of the plot of the displacement of the middle node in Figure 3.3, and introduce a couple of important definitions, initially introduced in [Carr et al., 2008].

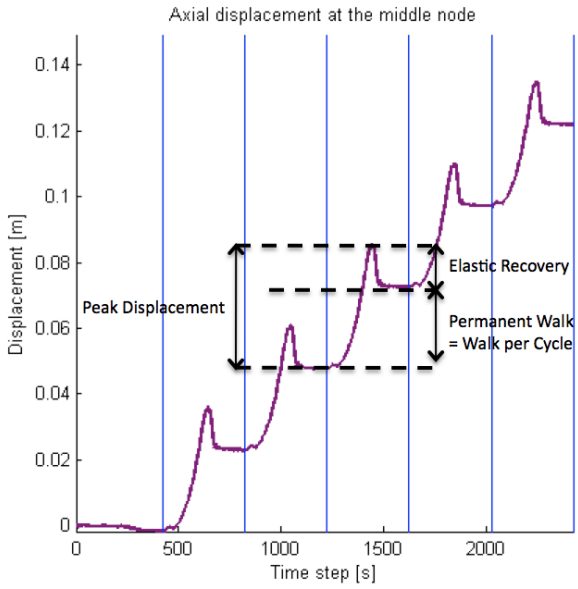

Figure 3.4: Detail of the Axial Displacement of the Middle Node of a Pipeline, with Definitions

The peak displacement illustrated in Figure 3.4 above is the maximum displacement the pipeline will undergo in the course of one cycle, before it contracts at cool-down. This contraction, which occur when the pressure and temperature decrease, is defined as the elastic recovery. When the cycle is at its' end, there has been a permanent walk. This permanent walk, occurring over one cycle, is referred to as the walk per cycle.

The earlier described long and short pipelines may also be categorized by a formula given in [Carr et al., 2008], with associated intervals for each. A third and intermediate case is also included in this categorisation, which is given in Equation 3.2

below.

$$\begin{aligned} \frac{f}{f^*} &< 1 \text{ for the short pipeline} \\ 1 < \frac{f}{f^*} &< 2 \text{ for the intermediate case} \\ \frac{f}{f^*} &> 2 \text{ for the long pipeline} \end{aligned} \tag{3.2}$$

where f is the effective axial friction force and $f^* = \frac{|\Delta P|}{L}$ is the friction force at which cyclic constraint occurs. ΔP is the fully constrained force, and L is the pipeline length.

One can see from Equation 3.2 that if the effective friction force is less than f^*, the pipeline is fully mobilised (i.e. short). For a pipeline to reach full constraint on first heat-up, the effective friction force must be larger than $2f^*$ (i.e. long). The intermediate case is described in [Carr et al., 2008] as the case where the fully constrained force is large enough to overcome the friction on first heat-up, but not on cool-down. This may lead to a cyclically constrained pipeline, which will vary its' behaviour dependant on where in the $\frac{f}{f^*}$ interval it is located. If it is close to 1, it will mostly resemble the behaviour of a short pipeline, while it will behave like a long pipeline if it is closer to 2.

The subjects outlined in this section have been based on the fact that the pipeline in question have been resting on a flat seabed, and have been subjected to constant temperature and pressure. In the following section several factors that may alter the rate of walking will be introduced.

3.3 Factors Influencing the Rate of Walking

In this section the factors influencing pipeline walking, which were introduced earlier in this chapter, will be outlined.

3.3.1 Thermal Gradients along the Pipeline

It has been mentioned earlier that when a pipeline walks, the movement is directed towards the cold end. In this subsection, this expression will be clarified, and the background for thermal loading will be introduced.

The direction of flow, and the resulting transients, decide the direction the pipeline walks. For this reason, it is important to take these into consideration when it comes to pipeline walking [Carr et al., 2008]. Figure 3.5 show the temperature

transients that the pipeline analysed in this thesis is subjected to. Details around this case study will be presented in Chapter 5.

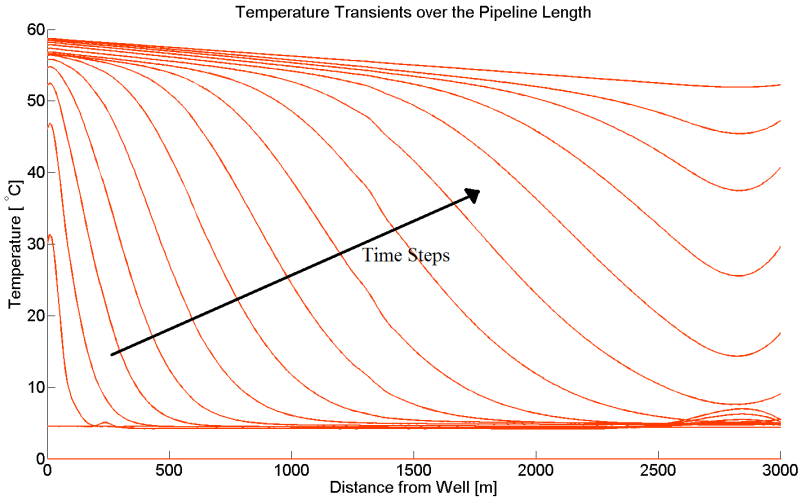

Figure 3.5: Distribution of the Temperatures over the Pipeline Length

The temperature transients are illustrated by the red lines shown in Figure 3.5. Each red line represent the collection of temperatures the pipeline is subjected to for each time step. The x-axis show the distance from the well, while the y-axis show the temperature. At the x-axis, x = 0 is closest to the wellhead, while x = 3000 is the point at the pipeline furthest from the wellhead. From the figure, it becomes clear that the hot end is closest to the wellhead, and the cold end is at the facility, or possibly the riser. The direction of walking is generally towards the cold end, i.e. towards the facility/riser.

The steepness of the thermal gradients is the key driver behind walking behaviour, especially the early stages of heat-up. In the early stages the cold end has not yet exceeded the ambient temperature. Another important factor is the shape of the thermal profile, which is developed over time as the pipeline heats up. The steeper the profile is, i.e. the higher the gradient, the more prone to walking the pipeline will be. If the thermal transient is extremely high, even a fully constraint section is not enough to keep the pipeline from walking [Carr et al., 2008].

3.3.2 The Seabed Conditions

The seabed conditions – which here translates to the pipe/soil interaction, and in particular the equivalent friction factor and the mobilisation length – have a great impact on the rate of walk per cycle. In [Tørnes et al., 2000] a sensitivity analysis

was performed, where both of these factors were assessed. It was found that the walk per cycle decreased as the mobilisation length increased. This corresponds with the description of the walking phenomena in Section 3.2, as well as the results found in [Carr et al., 2008].

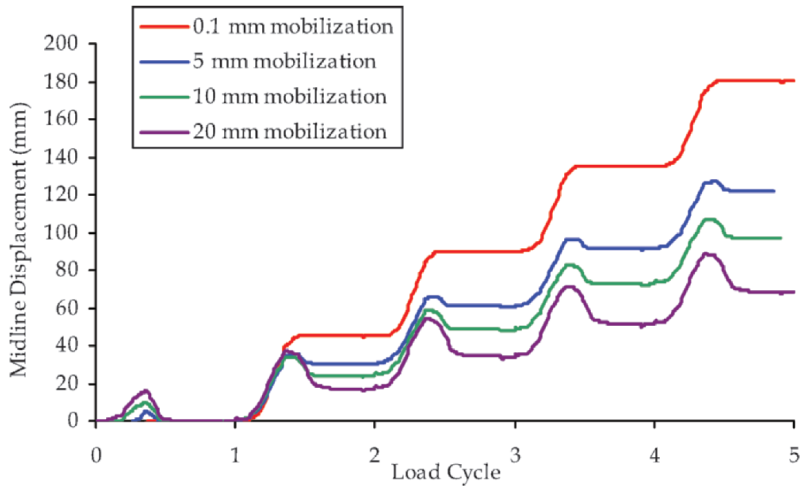

Figure 3.6: Effect of Mobilisation Length on Walking

Figure 3.6, provided by [Carr et al., 2008], show that the midline displacement increase with each cycle, as the mobilisation length decrease. In addition, the figure also show that the elastic recovery increase with increasing mobilisation length.

When it comes to the equivalent friction factor, [Tørnes et al., 2000] found that the walk per cycle increase as the equivalent friction factor increase, up to a certain point. After this point, the walk per cycle will decrease as the friction factor continue to increase. This can be seen in Figure 3.7, provided by [Tørnes et al., 2000].

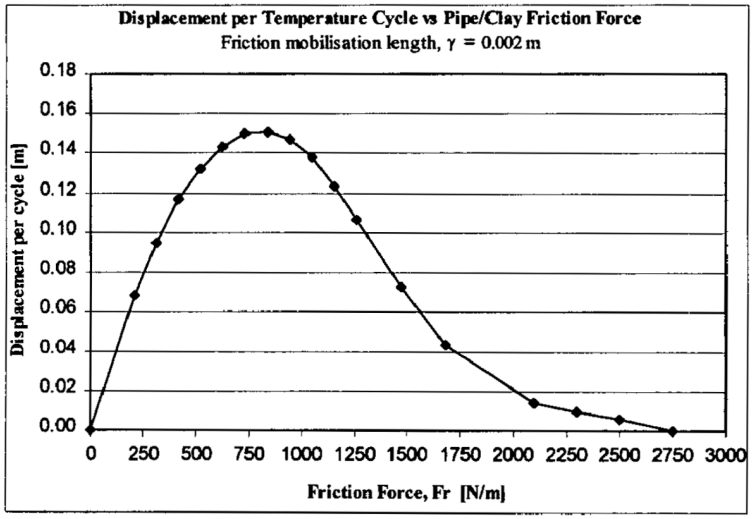

Figure 3.7: Walk per Cycle as a Function of the Friction Force

Here, the x axis show the pipe/clay friction force instead of for the friction factor, but the principle is still the same. The figure show several properties concerning the pipe/soil relationship. For very high friction factors, the pipeline will behave like a long pipeline, and be fully constrained. For low friction factors, the pipeline will become fully mobilised before the transients have had the time to pass along the pipeline. Thus, the pipeline stops walking before the whole pipeline is heated. The highest walk per cycle in this case is found to occur for $F_r \approx 840$ $[N/m]$ [Tørnes et al., 2000]. The highest walk per cycle occur when the pipeline reaches full mobilisation close to when the transient reaches the cold end of the pipeline [Carr et al., 2008].

The effect of change in the equivalent friction factor will be assessed in the case study in Chapter 5.

3.3.3 The Seabed Slope

A seabed slope, defined by an angle α along the pipeline's route can cause walking for each load cycle. The reason for this is that the pipeline weight acts in the direction of expansion. This will thus contribute to the walking – or counteract it – dependant on whether α is larger or smaller than zero. Figure 3.8, provided by [Carr et al., 2008], show the seabed slope sign convention.

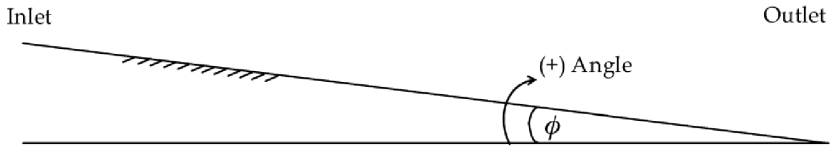

Figure 3.8: Seabed Slope Sign Convention

In the figure above, the angle is denoted ϕ, while the seabed angle will be denoted with α throughout the rest of this thesis. The inlet is the hot end of the pipeline, while the outlet is the cold end.

Figure 3.8 show a case where the weight of the pipeline will contribute to the walking. As a consequence, the global displacement of the pipeline will increase with an increasing angle.

The effect of a changing seabed slope will be assessed in the Case Study in Chapter 5.

3.3.4 Pipeline with Global Lateral Buckle

In this subsection a pipeline resting on a flat seabed with an initial global lateral buckle – a so called snake lay configuration – will be introduced, together with the theory describing this case.

When there is a buckle in the pipeline, the effective axial force decrease significantly. The reason for this is that the pipeline feeds axially into the buckle [Bruton et al., 2008]. This means that when the pipeline in question is subjected to increasing pressure and temperature, the direction of the expansion changes, i.e. the pipeline expands both towards the ends of the pipeline and into the buckle. In other words; the pipeline will still walk, but the global displacement will in total be smaller.

The effect of subjecting thermal transients to a pipeline with different initial buckles will be assessed in the case study in Chapter 5.

3.3.5 Tension Created by a Steel Catenary Riser

As mentioned earlier in this thesis, the cold end of the pipeline is the end in connection with the facility or riser. In deep water field developments a steel catenary riser (SCR) is usually the connection between the pipeline and the reception facility. The design of the SCR is so that it pulls the pipeline into tension at the SCR touch-down zone [Carr et al., 2008]. Figure 3.9, provided by [Brunner et al., 2006]

and amended to fit the case, show a floating production system (FPS) with a steel catenary riser connected to a pipeline at the SCR touch down point (TDP).

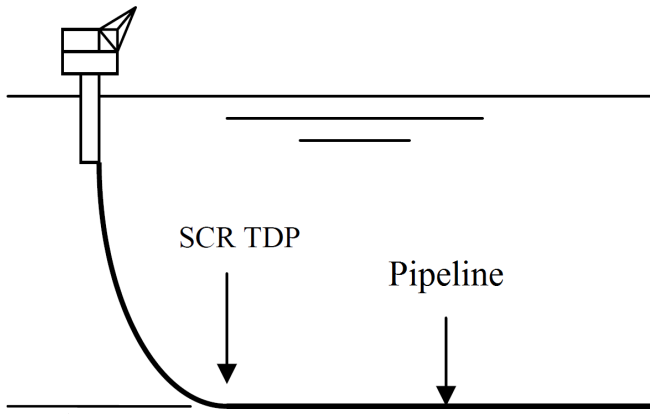

Figure 3.9: SCR and Pipeline

The introduction of this tension may cause the pipeline to walk under subsequent cycles. The tension applied by the SCR will vary, depending on the sea state conditions the FPS is subjected to. The tension from the SCR to the cold end of the pipeline will thus fluctuate with the period of the motion of the FPS.

The effect of linking a SCR to the cold end of a pipeline will be assessed in the case study in Chapter 5.

3.4 Walking Mitigation

It has been established earlier in this thesis that pipeline walking can lead to failures at tie-ins and risers. For this reason it is desirable to limit the extent of the large axial displacements walking can lead to. In [Perinet and Simon, 2011] it is stated that it is safer to provide mitigation measures to prevent pipeline walking than attempting to design the system so that the loads and displacements that would occur can be accommodated.

Hold-back anchors are commonly employed in the industry to control pipeline walking [Bruton et al., 2005]. This may however result in drawbacks for the overall design. When the pipeline goes through its' subsequent cycles, it also shuts down between the cycles. This induce additional tension due to the restraining anchors. For certain field layouts and routes, this may lead to lateral displacement [Bruton et al., 2005], and must thus be assessed in an early design stage.

Figure 3.10, provided by [Perinet and Simon, 2011], show an example of a mid-line anchor.

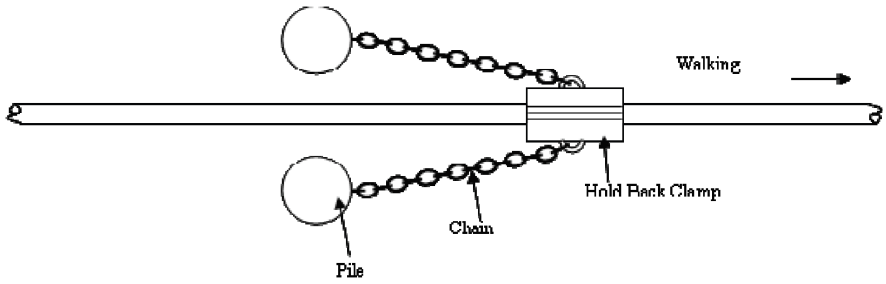

Figure 3.10: Anchor and Chain Restraint for a Pipeline

There are several ways to restrain the pipeline by anchors, and the above figure show one of them. It is also common to anchor the pipeline in its' ends. The anchor at the first end is quite practical to include in the system, since it is easily incorporated in the pipe laying process. However, anchoring the second end of the pipeline, in the process of terminating the pipe laying process, requires a more complex solution [Perinet and Simon, 2011]. According to [Bruton and Carr, 2011] the walking can be controlled by using anchors at the end from which the pipeline is walking. This solve the impracticalities related to the pipe laying process, although the pipeline would still be subjected to high levels of tension at shut-down.

Chapter 4

The SAFEBUCK JIP

As subsea pipelines are increasingly being required to operate at higher temperatures and pressures, the uncertainty around phenomena like pipeline walking and lateral buckling increase [Bruton and Carr, 2011]. The SAFEBUCK Joint Industry Project (SAFEBUCK JIP) was initiated to address these challenges.

Prior to this initiative the offshore industry witnessed a number of failures due to both lateral buckling and pipeline walking [Bruton and Carr, 2011], and there was a general agreement in the international pipeline industry to investigate these phenomena. The SAFEBUCK JIP was thus initiated in 2002 by Boreas Consultants, with contributions from Cambridge University and OTM Consulting. Boreas Consulting was acquired by Atkins in 2007, and Atkins has today the role as the JIP Lead [Atkins et al., 2013]. Several companies have joined the project throughout the years, and 18 companies are currently participants. Several of the methods and theories established through the JIP have been implemented in today's oil and gas projects [Atkins et al., 2013].

In this chapter the four stages in the JIP will be briefly introduced, and the parts relevant for the subjects in this thesis will be emphasised.

4.1 Phase I and II

The first two phases of the SAFEBUCK JIP resulted in the first design guideline for on-bottom lateral buckling, covering both single pipe and pipe-in-pipe pipelines. Analytical methods for assessing both lateral buckling and pipeline walking were established. In addition, several force-displacement response models for pipe/soil interaction were developed during Phase I of the JIP. These models are now used by the participants in the JIP to quantify the susceptibility to pipeline walking and lateral buckling [Bruton et al., 2008].

The knowledge from Phase I and II is captured in the SAFEBUCK Design Guideline [Atkins et al., 2013]. See also Figure 4.1 below, provided by [Bruton and Carr, 2011], which illustrate the scope of work performed to obtain the design guideline after Phase I.

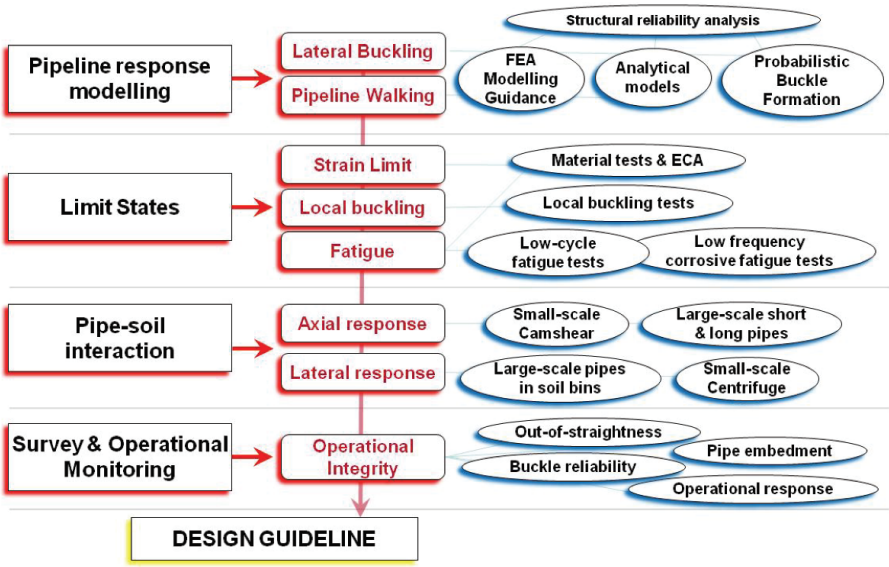

Figure 4.1: Scope of Work for the SAFEBUCK JIP Phase I

4.2 Phase III and Phase GEO

Phase III and Phase GEO of the SAFEBUCK JIP was run in parallel from the beginning of 2010.

The scope of work for Phase III contained a verification process of the reliability of the design methodology in the industry. The aim was to reduce over-conservatism in the design process. In addition, the formalisation of the SAFEBUCK Design Guideline into an Industry Recommended Practice was included in the scope of work [Atkins et al., 2013].

Phase GEO's scope of work contained a review of axial friction response, based on tests performed in the course of the JIP. By conducting this part, the aim was to improve the understanding of pipeline walking. As a continuation from Phase I, a new 'force-resultant plasticity model' was to be developed, with an aim to include this model in existing software packages that are used in the offshore pipeline industry today [Atkins et al., 2013].

4.3 Results from the SAFEBUCK JIP

The SAFEBUCK JIP have up to this day resulted in a design guideline for lateral buckling and pipeline walking, called the SAFEBUCK Design Guideline. This guideline is consistent with both of the current design codes DnV OS-F101 and API RP 1111, which are wideliy used in the industry today. In addition, several articles that enters into the core of the phenomena of both pipeline walking and lateral buckling have been produced. Many of these articles have been read in the course of working with this thesis, and some of these can be found in the Bibliography.

The aim of the JIP is to obtain a greater level of sharing of information from operating pipelines on recent projects in the industry, and to obtain a greater understanding of the challenges addressed. As long as this is done without sharing potentially sensitive project specific data, this is a mindset that all involved parties will benefit from.

When cooperating in exploring a phenomena like pipeline walking, and finding ways to address the challenges that follows this behaviour, the whole offshore pipeline industry will benefit from projects like the SAFEBUCK JIP.

Chapter 5

Case Study

The previous chapters in this thesis have been devoted to the theory of offshore pipeline technology, pipeline walking and a review of the SAFEBUCK JIP. This chapter will deal with the case study performed in the course of working with this master thesis. The aim of this case study have been to obtain a better understanding of the walking phenomenon with use of the MARINTEK software SIMLA.

The case study have consisted of a sensitivity analysis performed on a pipeline susceptible to walking. This pipeline scenario was defined in cooperation with the co-advisor from IKM Ocean Design (IKM OD). An earlier project, carried out by IKM OD, was used as a starting point. The final design data for the pipeline that was analysed can be found in Table 5.1 in Section 5.2. The thermal transients used in the case study was provided by the same project, and a presentation of these can be found in Section 5.2.2.

Oceanographic data, such as waves and current, have been neglected throughout this case study, with one exception. In the simulation of the SCR the period of the FPS have been included. This will be further described in Section 5.2.7.

5.1 Software and Programming Languages

Several computer programs and programming languages have been used in the course of working with this thesis, and these will be presented in this section.

5.1.1 SIMLA

SIMLA is a special purpose computer tool for engineering analysis of offshore pipelines during design, installation and operation. Bot a 2D and 3D FEM solu-

tion, each with its own associated degrees of freedom for each element in a linear and elastoplastic material model, is available [MARINTEK, 2013].

In this thesis SIMLA have been used to analyse each of the pipeline cases in the sensitivity analysis, which will be presented in the next section. This have been done by making use of implicit time integration on each equilibrium equation, which have been incrementally and dynamically solved in time and space.

Two input files, *autostart.sif* and *restart.sif*, have been used as a basis for each case in the case study. The input files have been amended to fit each case in the sensitivity analysis, and this will thus be described under the relevant sections in Section 5.2 in this chapter. The input files can be found under *\SIMLA* in the electronic appendix, which is separately enclosed. The SIMLA model used in the sensitivity analysis will be presented in Section 5.2.1.

5.1.2 FlexEdit and Xpost

FlexEdit and Xpost are two MARINTEK programs that are included in the utility package that follows the SIMLA software. FlexEdit is an editor, while Xpost is a visualisation program.

FlexEdit was in this thesis used to edit all the input files, as well as running SIMLA. Xpost was used to visualise the different cases, and extract relevant dynamic results.

5.1.3 MATLAB

MATLAB is a high-level language and interactive environment for numerical computation, visualisation and programming [MATLAB, 2013].

The results extracted from Xpost have been processed and plotted using MATLAB. These plots can mainly be seen in Chapter 6. MATLAB have also been used to plot the thermal transients. The walk per cycle in each case have also been calculated using MATLAB, and the results from these calculations can also be seen in Chapter 6, as well as in Appendix B. In addition, the analytical results have been calculated, plotted and compared to the results from SIMLA with the use of MATLAB. All MATLAB scripts can be found in the electronic appendix, which is separately enclosed.

5.1.4 Python and SciTE

Python is a dynamic programming language with an open source license, which is administered by the Python Software Foundation.

In this thesis Python 2.7 have been used, together with a couple of packages developed by IKM OD and the Python(x,y) package. SciTE is an editor that Python(x,y), and have been used to edit the python scripts. One script have been used to be able to run several SIMLA simulations within the same case consecutively, and another script have been used to plot the effective axial friction force diagrams. The scripts used can be found in the electronic appendix.

5.2 Sensitivity Analysis

The sensitivity analysis was performed on a 3000 [m] long pipeline with characteristics as shown in Table 5.1. The numerical values were provided by IKM OD, and thus given in [IKM, 20xx].

Characteristics	Information/Value	Dimension (if applicable)
Transported medium	Well stream	(N/A)
Pipe Material	Carbon steel with corrosion allowance	(N/A)
Internal Diameter (ID)	266.7	[mm]
Wall thickness	19.1	[mm]
Mean radius	142.9	[mm]
Outer Diameter (OD)	422.9	[mm]
Steel OD	304.9	[mm]
Corrosion Allowance	3.0	[mm]
Steel Grade	DNV SMLS 450 FPDU	(N/A)
Steel Density	7 850	[kg/m^3]
Young's Modulus @ 20 °C	207	[GPa]
Specified Minimum Yield Stress (SMYS) @ 20 °C	450	[MPa]
Specified Minimum Tensile Strength (SMTS) @ 20 °C	535	[MPa]
Material de-rating @ design temp	20	[MPa]
Poisson's Ratio	0.3	
Thermal Coefficient	1.17x10$^-$5	[1/°C]
Design Pressure, seabed level	307	[bar]
Design Temperature	78	[°C]

Table 5.1: Design data for the Given Pipeline

5.2.1 The SIMLA Model

To be able to perform the sensitivity analysis, the pipeline with characteristics as shown in Table 5.1 above, together with the seabed and sea surface, had to be modelled in SIMLA.

The pipeline model consists of beam elements, and the element type is defined as *pipe33*, which is a 3D element with constant axial strain and torsion. The material of the pipeline elements is defined as elastoplastic. The stress/strain relationship can be seen in Figure 5.1 below.

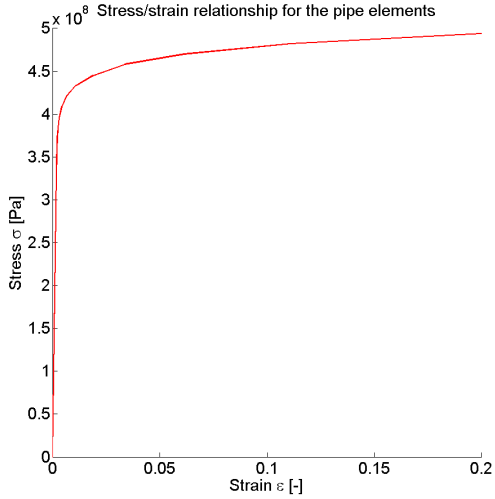

Figure 5.1: The Stress/strain Relationship for the Pipe Elements

The number of elements in the pipeline model was decided through an element sensitivity study, which is presented in Section 5.2.3 below.

The seabed model consists of elements of the type *cont126*, which is a 3D seabed contact element. A text file, containing information about water depth in, and xyz coordinates of, each point in the seabed, describes the nature of the seabed. The material of the seabed elements are defined by several sub-materials with both elastoplastic and hyperelastic behaviour. The connection between the pipe33 elements and the cont126 elements are modelled with springs.

The sea surface model consists of *sea150* elements, which are defined with a density of $\rho = 1026$ [kg/m^3].

Figure 5.2 below show the SIMLA model as it can be seen in Xpost. This is the so-called base case, which is the starting point for the sensitivity analysis.

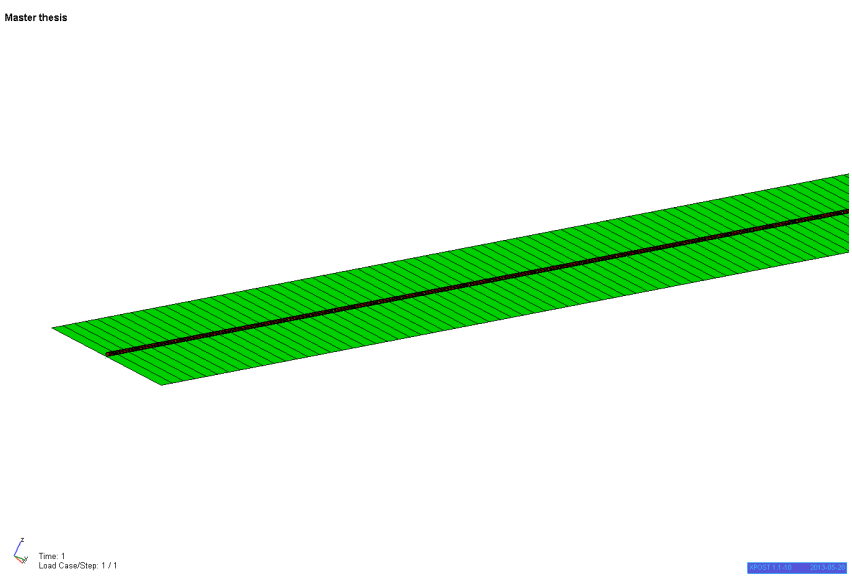

Figure 5.2: The SIMLA Model for the Base Case Shown in Xpost

5.2.2 Temperature Transients

The temperature transients were adopted from one of IKM's previous projects, so that the transients would be as authentic as possible. This was done by importing 363 text files into the SIMLA model, each containing a [322,2] matrix with time steps and the corresponding numerical value for the temperature.

The temperature files were evenly distributed over the elements, and these files can be seen the electronic appendix. Each file contain different numerical values for the temperatures, so that the heat transfer along the pipeline is represented. The temperature transients are illustrated in Figure 5.3 below.

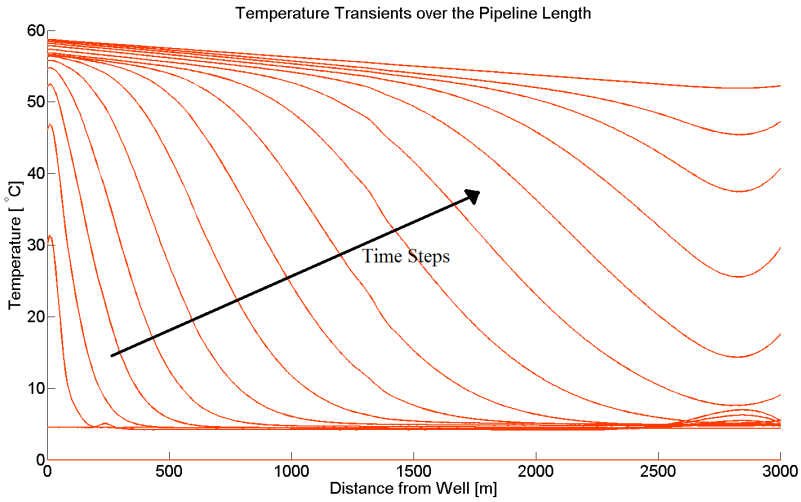

Figure 5.3: Distribution of the Temperatures over the Pipeline Length

Each line in Figure 5.3 above is the collection of the temperatures at one specific time step from each text file. 322 time steps with associated temperatures, of 8051 time steps in total, had been chosen to represent the temperature varying over the pipeline. The MATLAB script used to plot the temperature transients can be seen in the separately attached electronic appendix.

5.2.3 Element Length

To be able to assess the element length's impact on the simulations' running time, several element lengths were tested in SIMLA. The running time of one particular simulation will increase minimum fourfold when doubling the element length [Sævik, 2013]. Thus, it was considered important to find the optimum element length. The element lengths that was tested can be seen in Table 5.2 below.

Number of Elements	Element Length [m]
1 300	2.31
1 200	2.50
1 100	2.72
1 000	3.00
900	3.33
800	3.75
750	4.00

Table 5.2: Element Lengths

The model with 900 elements was considered to be the best choice for further simulations. The results and discussions that was the basis for this decision can be seen in Section 6.1.

5.2.4 The Seabed Conditions

As stated in Section 2.4, the pipe/soil interaction is of great importance when it comes to pipeline walking. To assess the effect of different seabed conditions, several simulations were run with different equivalent axial friction factors. These factors were based on Coulomb friction, and were included in the seabed elements' material definition. The Coulomb friction for the base case can be seen in Figure 5.4 below.

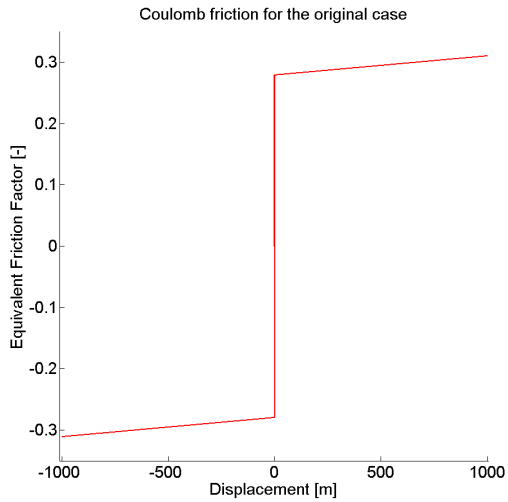

Figure 5.4: The Coulomb Friction for the Base Case

The numerical values for the equivalent friction factors included in the sensitivity analysis can be seen in Table 5.3, while the plots for $\mu_a = 0.1$, $\mu_a = 1.1$ and $\mu_a = 2.1$ can be seen in Figure 5.5.

Equivalent Friction Factors	0.1	0.2	0.3	0.4	0.5	0.6	0.7	0.8	0.9	1.0	1.1
	1.2	1.3	1.4	1.5	1.6	1.7	1.8	1.9	2.0	3.1	2.2

Table 5.3: The Equivalent Friction Factors Included in the Sensitivity Analysis

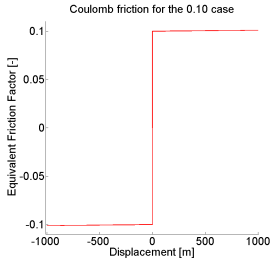

(a) Coulomb Friction Diagram for $\mu_a = 0.1$

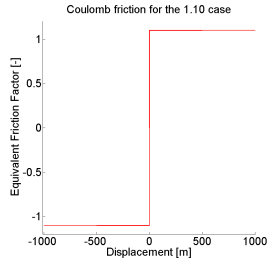

(b) Coulomb Friction Diagram for $\mu_a = 1.1$

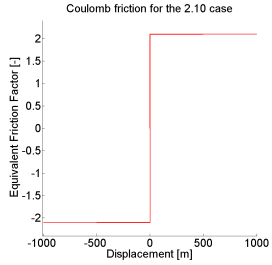

(c) Coulomb Friction Diagram for $\mu_a = 2.1$

Figure 5.5: The Coulomb Friction for Three of the Cases in the Sensitivity Analysis

The results from the seabed conditions analysis can be found in Section 6.3.

5.2.5 The Seabed Slope

To assess the influence of a changing seabed slope on pipeline walking, several seabed angles were included in the SIMLA simulations. This was done by importing different route files into the seabed configuration.

The route files were modified by changing the depth along the pipeline length, and thus increasing or decreasing the seabed slope. The seabed angles that were included in this part of the sensitivity analysis, as well as the associated start and end depths, can be seen in Table 5.4. The relevant route files can be seen in the separately attached electronic appendix under *\SIMLA\Route Files*.

Seabed Angle α [°]	Depth at Node 1 [m]	Depth at Node 901 [m]
-2.5	300.29	130.00
-2.0	266.25	130.00
-1.5	232.19	130.00
-1.0	198.13	130.00
-0.5	164.07	130.00
0.0	130.00	130.00
0.5	130.00	164.07
1.0	130.00	198.13
1.5	130.00	232.19
2.0	130.00	266.25
2.5	130.00	300.29

Table 5.4: Seabed Slope Values

The new depths were found by the use of the principles shown in Figure 5.6, and the formula shown in Equation 5.1.

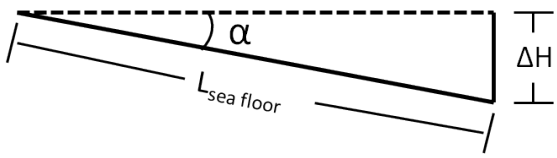

Figure 5.6: Principles for Calculating the New Depths of the Sea Floor

$$H_{new} = H + L_{seafloor} \sin \alpha \tag{5.1}$$

Here ΔH is the change in depth, and H_{new} is the new depth either at Node 1 or Node 901, to obtain the seabed angle α. H is the original depth of 130 [m], and $L_{seafloor}$ = 3 903.94 [m] is the length of the sea floor included in the seabed model.

Figure 5.6 above is equivalent to Figure 3.8, previously shown in Section 3.3.3. The hot end/inlet is to the left, while the cold end/outlet is to the right in both figures, which is valid for $\alpha > 0$. For $\alpha < 0$, the hot and cold end switch places, i.e. the inlet is at the bottom of the slope.

After running simulations with the angles in Table 5.4, it was decided to run simulations for the angles in the following table as well.

Seabed Angle α [°]
-0.40
-0.45
-0.50
-0.55
-0.60

Table 5.5: Seabed Slope Values for the Detailed Case

The reason for including the angles in Table 5.5 in the case study as well will be presented in Section 6.4, together with all the results from the seabed slope sensitivity analysis.

Analytical Solution

In agreement with the supervisor it was decided to use an analytical model from the literature [Sævik, 2013], and in [Carr et al., 2008] an analytical model for the seabed slope case is presented. The starting point for this model is presented in Figure 5.7 below.

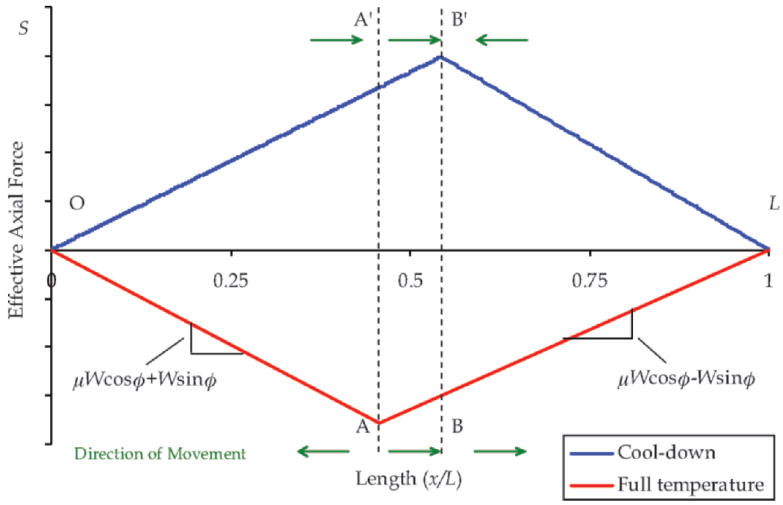

Figure 5.7: Force Profile for Sloping Seabed

The walk per cycle can then be calculated by Equation 5.2, 5.3, 5.4, 5.5 and 5.6 introduced below.

The length between the virtual anchors can be calculated by

$$X_{ab} = \frac{L \tan \alpha}{\mu_a} \tag{5.2}$$

where X_{ab} is the length between the virtual anchor points, L [m] is the pipeline length, α [deg] is the angle of the seabed and μ_a [-] is the equivalent axial friction factor. The change in axial force in the pipeline ΔS_s [N] over the length X_{ab} [m] is given by

$$\Delta S_s = -WL(\mu_a \cos \alpha - |\sin \alpha|) \tag{5.3}$$

where W is the submerged unit weight [N/m] of the pipeline. The change in fully constrained axial force is given by

$$\Delta P = -(p_{i,2} - p_{i,1})A_i(1 - 2\nu) - EA_s\kappa(\theta_2 - \theta_1) \tag{5.4}$$

where ΔP is the change in fully constrained axial force, p_i is the internal pressure [Pa], A_i is the cross sectional area of pipe inside diameter [m^2], ν is the Poisson's Ratio, E is the Young's Modulus [N/m^2], κ is the coefficient of thermal expansion [$1/°C$] and θ is the operating temperature [$1/°C$]. The change in axial strain is given by

$$\Delta\epsilon = \frac{\Delta S_s - \Delta P}{EA} \tag{5.5}$$

where $\Delta\epsilon$ is the change in axial strain. Based on the equations above, the walk per cycle caused by a seabed slope is given by

$$\Delta_\alpha = \frac{[|\Delta P| + WL|\sin\alpha| - WL\mu_a\cos\alpha]L\tan\alpha}{\mu_a EA} \tag{5.6}$$

where Δ_α is the walk per cycle.

The analytical solution for the seabed slope case will be compared to the corresponding results from SIMLA in Section 6.4.

5.2.6 Pipeline with Global Lateral Buckle

To assess the effect a global lateral buckle in the pipeline may have on pipeline walking, eight cases were analysed. In these cases both radius and length of the curve was varied. In Figure 5.8 below two of the cases, shown in Xpost, is presented.

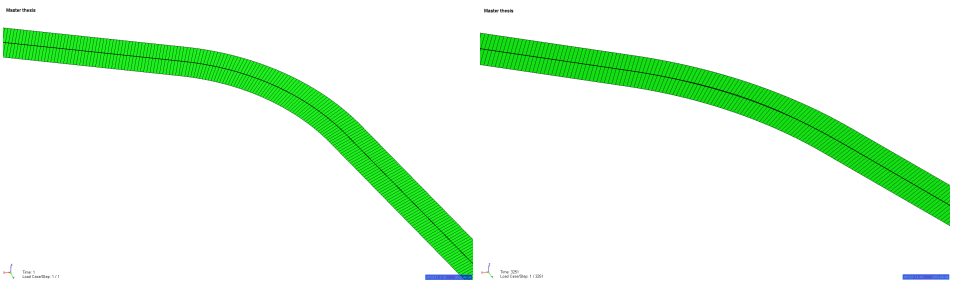

(a) The Pipeline with 250 [m] Radius and 200 [m] Curve Length

(b) The Pipeline with 400 [m] Radius and 200 [m] Curve Length

Figure 5.8: Two of the Pipelines Tested in the Global Lateral Buckle Analysis

Table 5.6 below show the properties of the eight cases that were analysed in this part of the sensitivity analysis.

Radius [m]	Curve Length [m]
250	50
	100
	150
	200
400	50
	100
	150
	200

Table 5.6: Seabed Slope Values for the Detailed Case

The buckles in the pipelines were included by changing the route file in every case, and thus implementing the buckles in the SIMLA model. The route files were generated by using Python, and the relevant script can be found in the separately attached electronic appendix. The route files can be seen in the electronic appendix under *\SIMLA\Route Files*. See also Figure 5.9 and Figure 5.10, which show the plotted route files for the same cases that were shown in Figure 5.8 above.

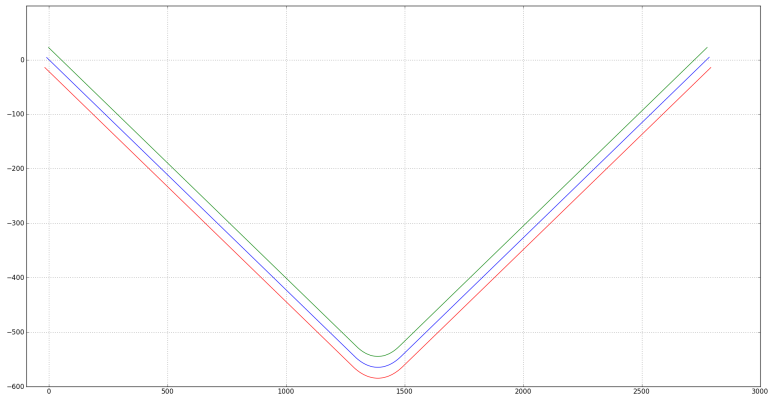

Figure 5.9: The Plotted Route of The Pipeline with 250 [m] Radius and 200 [m] Curve Length

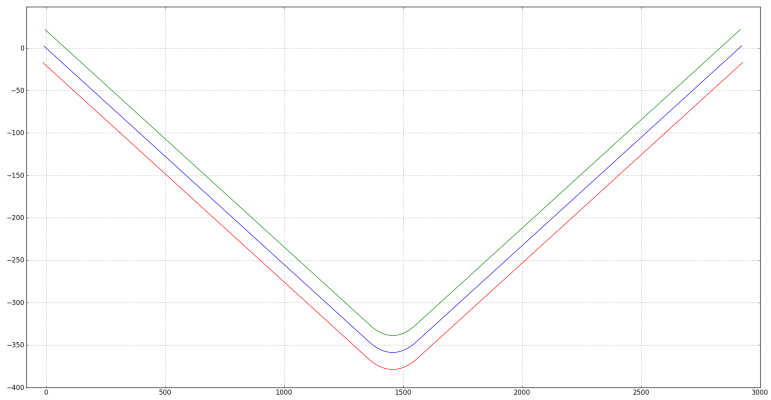

Figure 5.10: The Plotted Route of The Pipeline with 400 [m] Radius and 200 [m] Curve Length

To be able to isolate the walking behaviour, the pipeline model was only allowed to move in the local axial direction. Still, the pipeline was free to move both laterally and axially in the buckle.

The results from the global buckle analysis can be found in Section 6.5 in Chapter 6.

5.2.7 Tension Created by a Steel Catenary Riser

To be able to assess the effect a SCR could have on pipeline walking, two simulations were run in SIMLA; one case with a SCR, and one case without a SCR. The last case corresponds to the base case.

After conversations with [Sævik, 2013] it was decided to apply an oscillating load at the cold end of the pipeline, i.e. node 901 in the pipeline model. The load factor is defined in Equation 5.7, given by [Sævik et al., 2012].

$$F = \sin(\omega t + \phi) \tag{5.7}$$

Here, ω is the frequency of the assumed FPS, and ϕ is the phase displacement. The tension load from the SCR was decided to have an amplitude corresponding to 10% of the lay tension, i.e. 5 [kN], and a period of 10 [s]. This give

$$\omega = \frac{2\pi}{T} = \frac{2\pi}{10} = 1.97[rad/s]$$

The phase displacement ϕ was set to zero. To be able to isolate the walking behaviour, the pipeline model was only allowed to move in the local axial direction.

The results from the SCR analysis will be discussed in Section 6.6 in Chapter 6.

Analytical Solution

In agreement with the supervisor it was decided to use an analytical model from the literature [Sævik, 2013], and in [Carr et al., 2008] an analytical model for the SCR case is presented. As for the seabed slope case, the starting point for this model is presented in Figure 5.11 below.

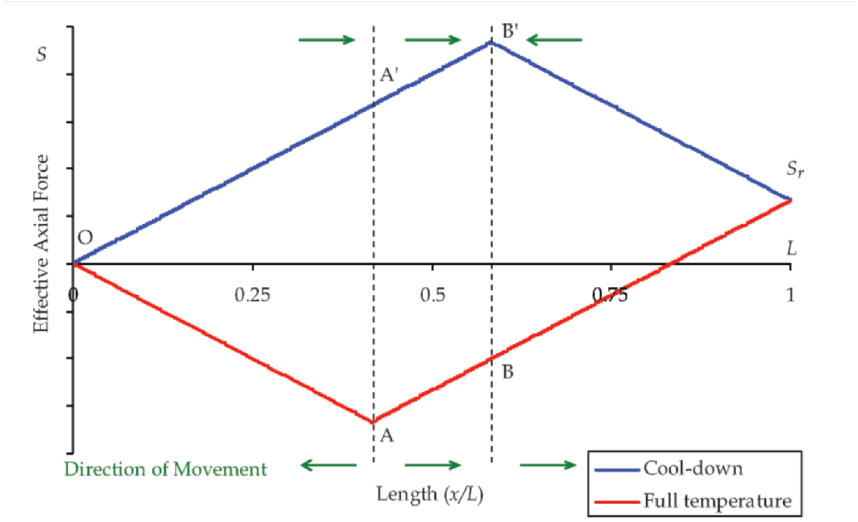

Figure 5.11: Force Profile for SCR at the Cold End

The walk per cycle can then be calculated by Equation 5.8, 5.9, 5.10, 5.11 and 5.12 introduced below.

The length between the virtual anchors can be calculated by

$$X_{ab} = \frac{S_R}{f} \tag{5.8}$$

where X_{ab} is the length between the virtual anchor points, S_R is the tension due to the SCR and f is the effective axial friction force. The change in axial force in the pipeline ΔS_f over the distance X_{ab} is given by

$$\Delta S_f = S_R - Lf \tag{5.9}$$

where L is the pipeline length. The change in fully constrained axial force is given by

$$\Delta P = -(p_{i,2} - p_{i,1})A_i(1 - 2\nu) - EA_s\kappa(\theta_2 - \theta_1) \tag{5.10}$$

where ΔP is the change in fully constrained axial force, p_i is the internal pressure [Pa], A_i is the cross sectional area of pipe inside diameter [m^2], ν is the Poisson's Ratio, E is the Young's Modulus [N/m^2], κ is the coefficient of thermal expansion [$1/°C$] and θ is the operating temperature [$1/°C$]. The change in axial strain is given by

$$\Delta\epsilon = \frac{\Delta S_s - \Delta P}{EA} \tag{5.11}$$

where $\Delta\epsilon$ is the change in axial strain. Based on the equations above, the walk per cycle caused by a SCR is given by

$$\Delta_R = \frac{(|\Delta P| + S_R - fL)S_R}{EAf} \tag{5.12}$$

where Δ_α is the walk per cycle.

The analytical solution for the SCR case will be compared to the corresponding results from SIMLA in Section 6.6.

Chapter 6

Results and Discussion

In this chapter the results from the case study, which was described in the previous chapter, will be presented and discussed.

6.1 The Element Length

Several analyses were run to assess the impact element length would have on the walking results, and thus determine a base case for further analyses. The computational time for each element length is listed in Table 6.1 below.

Number of Elements	Element Length [m]	Time [s]	Time [min]	Time [h]
1 300	2.31	20 237	337.28	5.62
1 200	2.50	18 291	304.85	5.08
1 100	2.72	16 943	282.38	4.71
1 000	3.00	21 543	359.05	5.98
900	3.33	14 526	242.1	4.04
800	3.75	2 336	38.93	0.65
750	4.00	1 621	27.02	0.45

Table 6.1: Element Length versus Simulation Time

The results concerning the simulation time used may be affected by external factors, such as other users of the computer also running analyses. Still, the time used give an impression of how time consuming each simulation is. There is an

evident jump in time used from 900 to 800, and down to 750 elements. In contrast, the computational time steadily increase, and even slightly decrease for one case, from the model with 900 elements and upwards.

Figure 6.1 below show the displacement of the middle node over 12 cycles for each of the analysis models. The blue, vertical lines represent the starting point for each cycle.

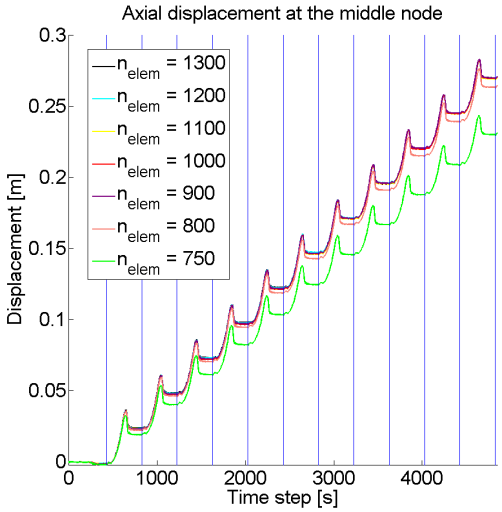

Figure 6.1: Axial Displacement of the Middle Node with Varying Element Length

By studying the figure above the results from Table 6.1 become more comprehensible. The models with 900 elements and above have the same progress over the twelve cycles, and they thus converge. In contrast, the solutions for 750 and 800 elements do not follow the same pattern, which means that they do not converge towards the same result. Table 6.2 below show the same tendencies, when presenting the walk per cycle in each case.

Number of Elements	Walk per Cycle [m]
1 300	0.024630
1 200	0.024636
1 100	0.024610
1 000	0.024730
900	0.024704
800	0.024118
750	0.021105

Table 6.2: Element Length and Walk per Cycle

Additional three SIMLA models, with up to 1 600 elements, were tested. These results were showed the same tendencies, and are therefore not included here.

According to [Sævik, 2013] the element length should have a value between 2.5 and 5 times the diameter of the pipeline. In this case this would result in an element length between 1.06 [m] and 2.11 [m], which would call for minimum 1422 elements. However, since the walk per cycle in each case seem to converge towards the same value for 900 elements and upwards, the 900 element model was chosen for further analyses due to lower computational time. This choice was taken after consulting with [Sævik, 2013], and in the search for gaining a larger insight into the walking phenomenon, this model was regarded as acceptable.

6.2 Development of the Effective Axial Friction Force

Figure 6.2 below show the development of the effective axial friction force through the second heat-up cycle.

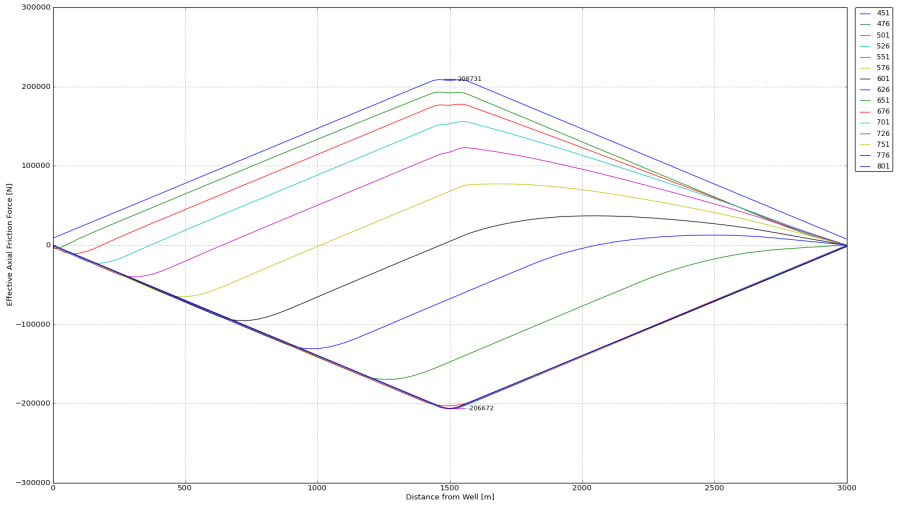

Figure 6.2: Effective Axial Friction Force Development in the First Heat Up for the Base Case

The top blue line, labelled 451, is the effective axial friction force at the cool-down step from the previous cycle. The green line, just below the blue one, is the first effective axial friction force at the first warm-up down step in the second cycle. The subsequent lines show the further development of the effective axial friction force. The figure can be seen in context with the temperature transients, which can be seen in Figure 5.3, in the previous chapter. The temperature transients are regarded as the driving factor behind this case.

6.3 The Seabed Conditions

To assess the effect of a changing equivalent friction factor in the axial direction, 22 cases were simulated in SIMLA. Figure 6.1 and Figure 6.4 below show the results from the seabed conditions sensitivity study.

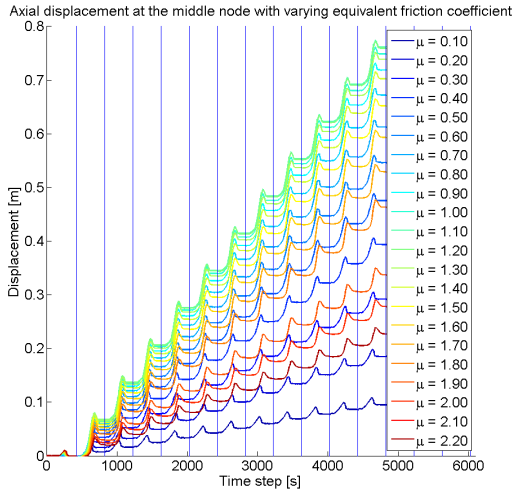

Figure 6.3: Axial Displacement of the Middle Node with Varying Equivalent Friction Factor

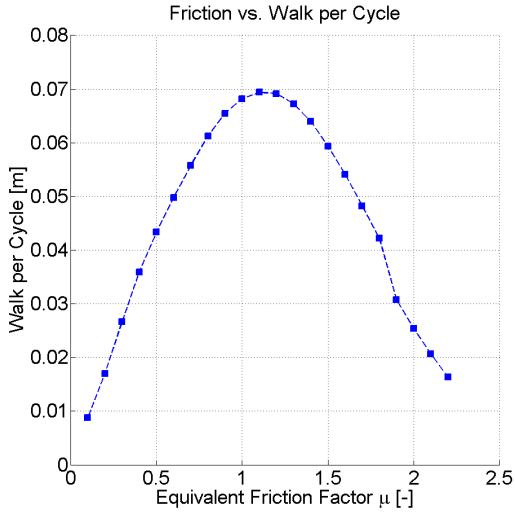

Figure 6.4: Equivalent Friction Factor Plotted against Walk per Cycle

Both Figure 6.3 and Figure 6.4 show the tendencies previously presented in Section 3.3.2; the walk per cycle increase as the equivalent friction factor increase, up to $\mu_a = 1.1$, before the walk per cycle decrease as the equivalent friction factor continue to increase.

To be able to study this behaviour qualitatively, the effective axial friction forces diagrams for three of the seabed condition cases will be presented. These are $\mu_a = 0.1$, $\mu_a = 1.1$ and $\mu_a = 2.1$, and the diagrams can be seen in Figure 6.5, Figure 6.6 and Figure 6.7, respectively. The figures show the effective axial friction force for all twelve cycles, on heat-up an cool-down. The compressive forces occur on heat-up, while the tensile forces occur on cool-down. All effective axial friction force diagrams for this case can be found in Appendix A.1.

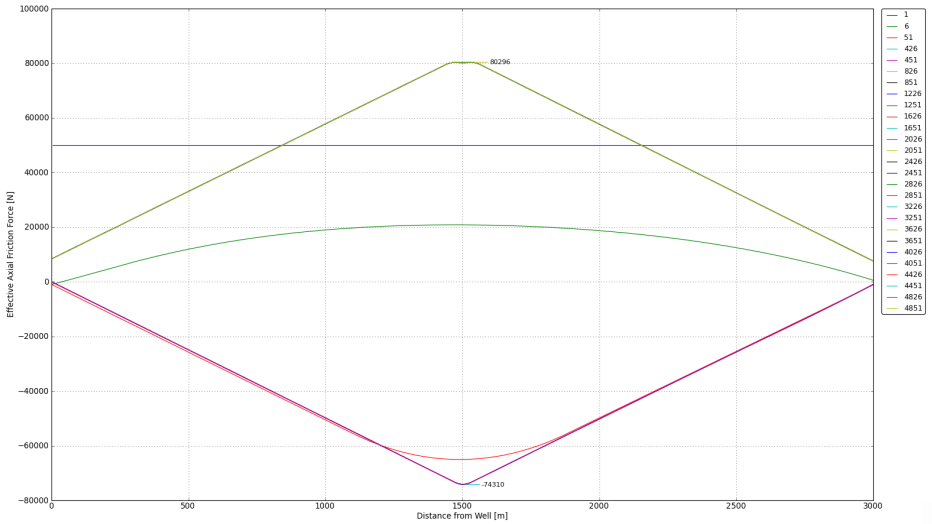

Figure 6.5: Effective Axial Friction Force for $\mu_a = 0.1$

The diagram in Figure 6.5 above agrees quite well with corresponding diagrams in the literature. This case appear to coincide with the theory presented in Section 3.3.2; for a small μ_a the pipeline will be fully mobilised before it is properly heated, and the walking comes to an halt.

The mid value in Figure 6.5 is not as peaked as for analytical diagrams, which is due to the material configuration in the seabed model in SIMLA. As earlier stated, the contact between the pipeline and seabed is modelled with springs. This give this rounded peak of the maximum effective axial friction force.

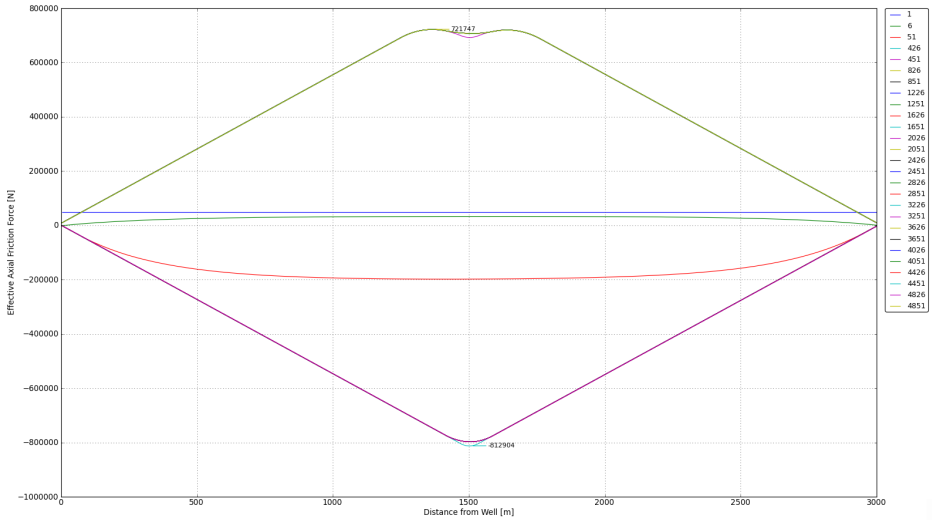

Figure 6.6: Effective Axial Friction Force for $\mu_a = 1.1$

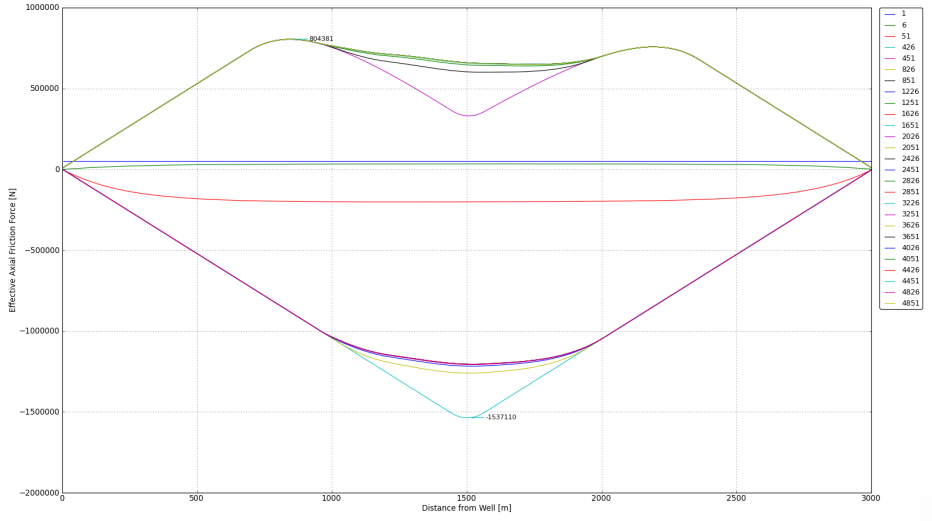

Figure 6.7: Effective Axial Friction Force for $\mu_a = 2.1$

The three figures above show the development of the effective friction force for increasing effective friction factor. The diagram for the $\mu = 2.1$ case resemble the diagrams for cyclically constrained pipelines, which were introduced in Section 3.2.

For an increasing equivalent friction factor two virtual anchors develop, and move towards the pipeline ends. In other words, for an increasing equivalent friction factor, the anchor length decrease.

Between the two virtual anchor points, the pipeline does not reach full mobilisation. This means that the pipeline/soil behaviour only act in the elastic area of the axial friction curve (with reference to Figure 5.5c in the previous chapter) for this part of the pipeline. Consequently, the effective friction force does not move from maximum compression to maximum tensile as soon as the cool-down start. Thus, there is a large friction force available, and the middle section of the pipeline only operate in the elastic section of the soil material curve.

6.4 The Seabed Slope

Five positive, and five negative angle values were chosen, and the related SIMLA models created. The simulations were run, and the results from the seabed slope case is thus presented in this section.

The displacement of the middle node of the pipeline for each of the positive seabed angle values can be seen in Figure 6.8, while displacement of the middle node of the pipeline for each of the negative seabed angle values can be seen in Figure 6.9.

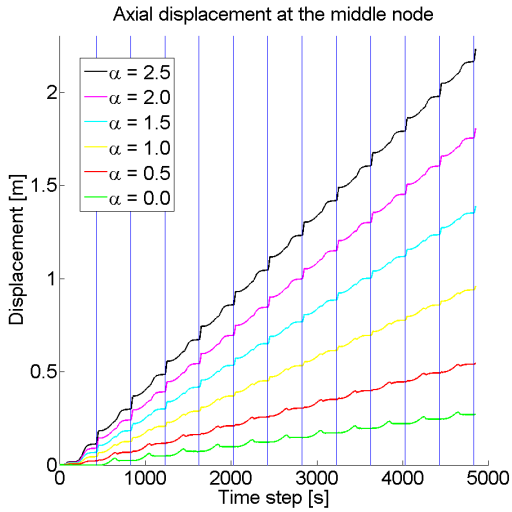

Figure 6.8: Axial Displacement of the Middle Node for Positive Angles

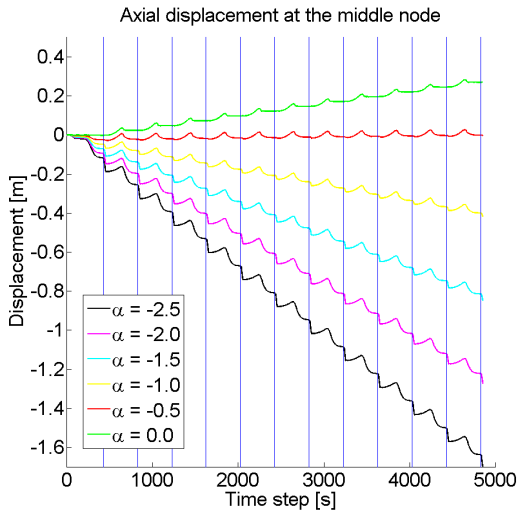

Figure 6.9: Axial Displacement of the Middle Node for Negative Angles

The two figures above show the development of the walking displacement, over the 12 cycles, as the angle increase in value. One can note that when the negative angle increase to a certain point in absolute value, the pipeline appear to walk towards the hot end. This indicate that for a steeper seabed slope, the seabed slope will have a greater impact on the walking phenomenon than the temperature transients.

The walk per cycle plotted against the angles for each of the positive seabed angles can be seen in Figure 6.10, while the walk per cycle plotted against the angles for each of the negative seabed angles can be seen in Figure 6.11.

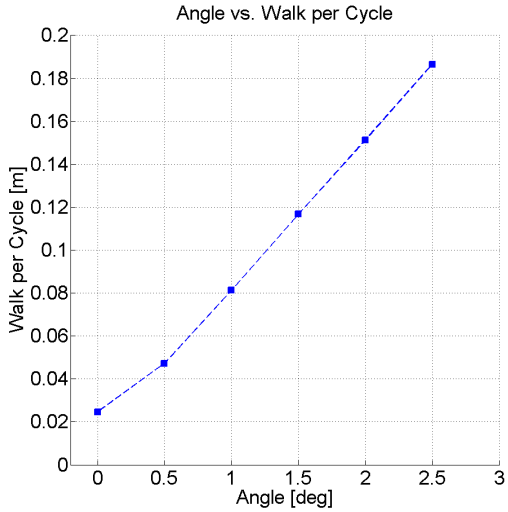

Figure 6.10: Walk per Cycle Plotted Against Positive Angles

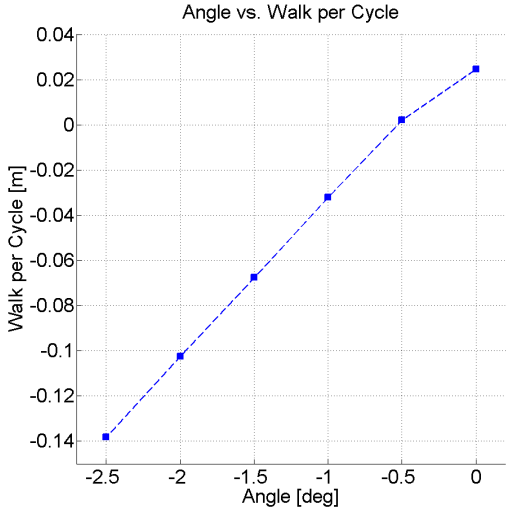

Figure 6.11: Walk per Cycle Plotted Against Negative Angles

Figure 6.10 and Figure 6.11 show that the relationship between the increasing angle and increasing walk per cycle is almost linear. The deviation seem to originate from the $\alpha = 0.0$ case, which corresponds to the base case.

Based on the above four figures, the α = -0.5 case will be further studied. This is

the case where the walk per cycle is closest to zero, and this boundary area is thus eligible to further assessment. A more detailed case was created, and the results for this case can be seen in Figure 6.12 and Figure 6.13 below.

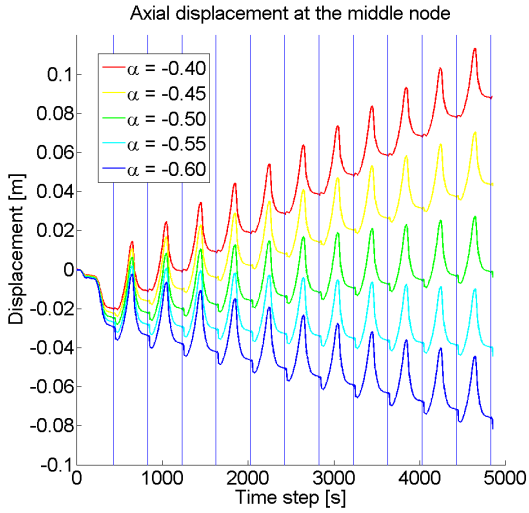

Figure 6.12: Axial Displacement of the Middle Node for the Detailed Case

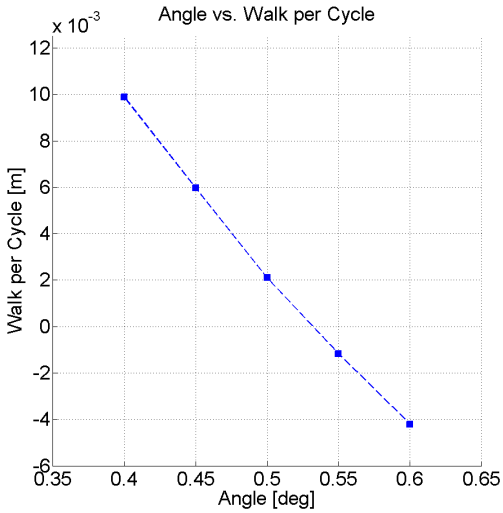

Figure 6.13: Walk per Cycle Plotted Against Negative Angles in the Detailed Case

The two figures above show that the α = -0.50 and α = -0.55 cases have the smallest walk per cycle. The exact numerical values are given in Table 6.3 below. The walk per cycle values for all the cases can be found in Appendix B.1.

Angle [deg]	Walk per Cycle [m]	Walk per Cycle [mm]
α = -0.50	0.0021	2.1
α = -0.55	-0.0012	1.2

Table 6.3: Walk per Cycle for α = -0.50 and α = -0.55

The table above show that the walk per cycle is smallest for the α = -0.55 case. This may also be regarded as the turning point for the seabed slope case. In this area the effect from the increasing seabed slope have a greater impact on the walking behaviour than the temperature transients. In other words the walking movement shifts, and the pipeline will walk towards its' hot end.

The effective axial friction force for α = -0.50 and α = -0.55 are shown in Figure 6.14 and Figure 6.15 below. The rest of the effective axial friction force diagrams can be found in Appendix A.2.

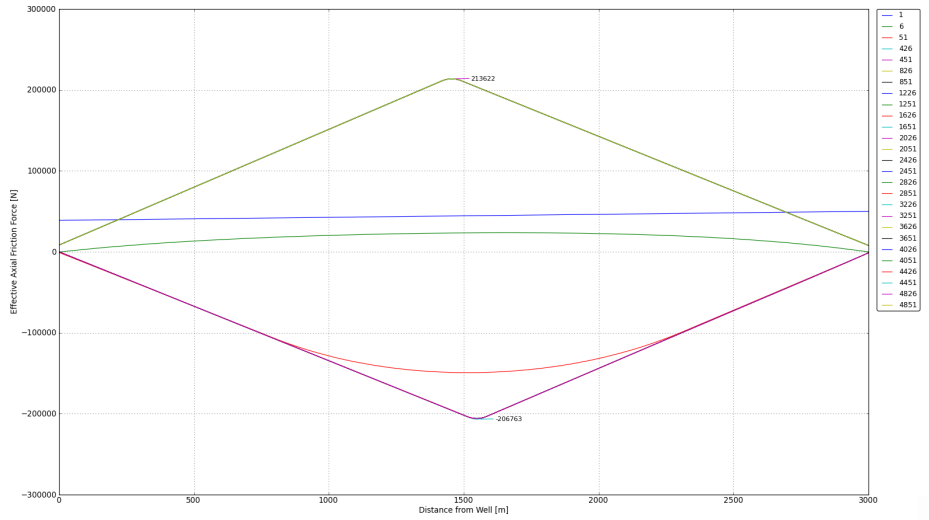

Figure 6.14: Effective Axial Friction Force for α = -0.50

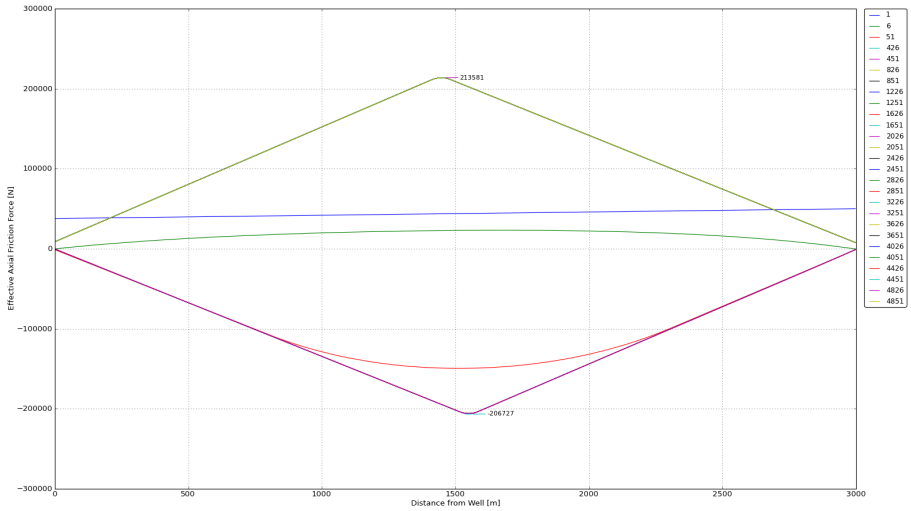

Figure 6.15: Effective Axial Friction Force for α = -0.55

The two diagrams in the figures above are almost identical, although the pipe walk towards the cold end in the first case and towards the hot end in the second case. The shape of the diagram, with the top point towards the left and the bottom point towards the right, show that the seabed slope angle is negative. This imply that on a sloping seabed it is not possible to tell if the pipeline is walking towards the hot or cold end simply based on the effective axial friction force diagrams. However, if the pipeline had not been subjected to temperature transients in addition to the seabed slope, this could have been possible. This is shown in the next section.

Analytical Results

The results from the seabed slope case were compared to analytical results, by using equations presented in the literature. These can be found in Section 5.2.5 in the previous chapter.

The walk per cycle for each angle, for both positive and negative angles, for the numerical and analytical solutions are presented in Figure 6.16 and Figure 6.17 below.

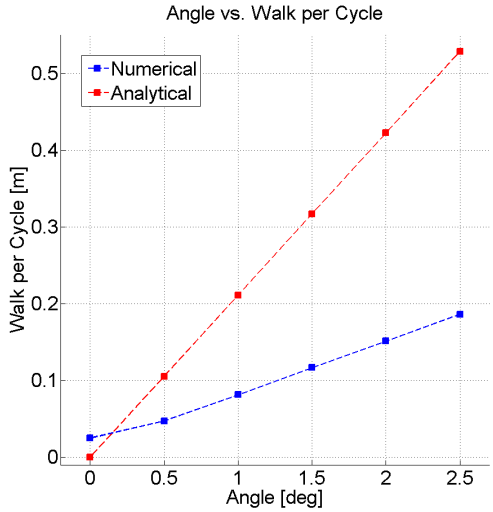

Figure 6.16: Walk per Cycle Plotted Against Positive Angles for both the Analytical and Numerical Solutions

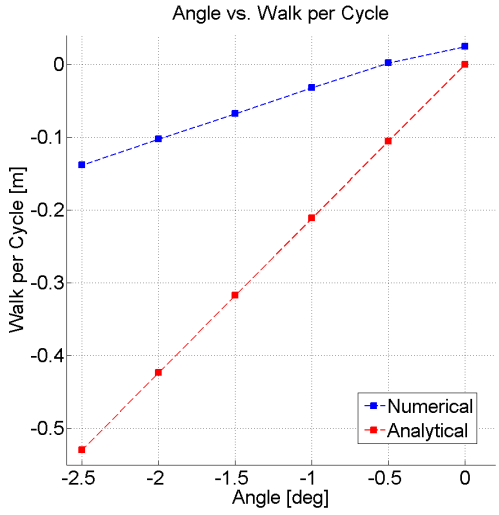

Figure 6.17: Walk per Cycle Plotted Against Negative Angles for both the Analytical and Numerical Solutions

The figures show that there is a difference between the numerical and analytical results, and the deviation increase for an increasing seabed slope. The numerical values, and the deviation presented per cent wise, can be found in Table 6.4 below.

Angle [deg]	Walk per Cycle [m] Analytical Solution	Walk per Cycle [m] Numerical Solution	Deviation [m]	Deviation [%]
$\alpha = 0.0$	0.0000	0.0247	0.0247	100
$\alpha = 0.5$	0.1055	0.0472	0.0583	55.26
$\alpha = 1.0$	0.2111	0.0813	0.1298	61.49
$\alpha = 1.5$	0.3169	0.1168	0.2001	63.14
$\alpha = 2.0$	0.4229	0.1513	0.2716	64.22
$\alpha = 2.5$	0.5292	0.1865	0.3427	64.76
$\alpha =$ -0.5	-0.1055	0.0021	0.1076	51.24
$\alpha =$ -1.0	-0.2111	-0.0320	0.1791	84.84
$\alpha =$ -1.5	-0.3169	-0.0676	0.2493	78.67
$\alpha =$ -2.0	-0.4229	-0.1025	0.3204	75.76
$\alpha =$ -2.5	-0.5292	-0.1382	0.3910	73.89

Table 6.4: Analytical and Numerical Solutions

As the table and figures above show, the difference between the numerical and analytical solutions are quite large. This may have several reasons, and these will be presented in the following paragraph.

The analytical model presented in [Carr et al., 2008] are only subjected to the increasing/decreasing slope, while the SIMLA model is subjected to both a seabed slope and thermal transients. This may explain why there is walking for $\alpha = 0.0$ for the SIMLA model, but not for the analytical model. The $\alpha = 0.0$ case corresponds to the base case. If the only reason for the differences between the two result were the thermal transients, the graphs in Figure 6.16 and Figure 6.17 should have been approximately parallel. However, the difference increase as the angle increase. This may be so because the analytical model is more conservative than the SIMLA model, and as a result the analytical model has a much steeper walk per cycle curve than the numerical model.

6.5 Pipeline with Global Lateral Buckle

Eight SIMLA models were created for assessing the effect of a global lateral buckle on pipeline walking. The displacements for each of the cases can be seen in Figure 6.18 below.

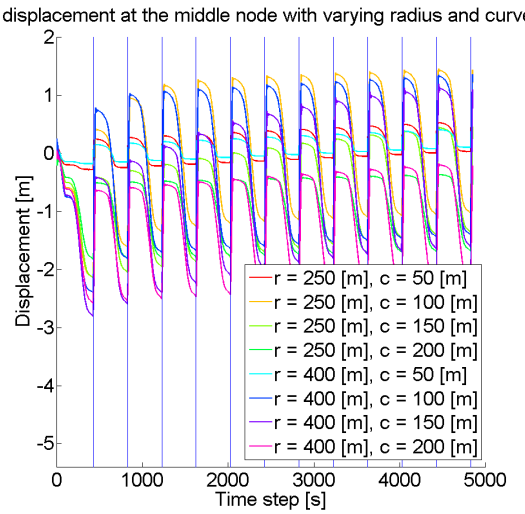

Figure 6.18: Axial Displacement of the Middle Node for the Global Lateral Buckle Case

The figure above show that the axial movement for each case is quite large, but that the total displacement is not. This means that the peak displacement and elastic recovery is large in each cycle, but that the permanent walk is relatively small. The large peak displacement may seem to confirm the theory presented in Section 3.3.4, which stated that the displacement will feed into the buckle, and thus not walk as much as for the base case.

The walk per cycle is plotted against the curve length in Figure 6.19 below, with one graph for each radius.

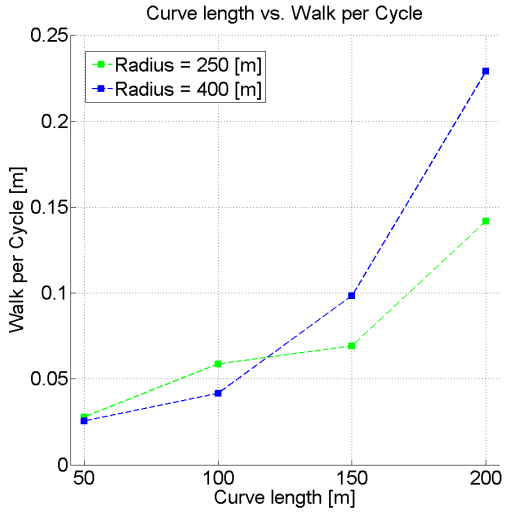

Figure 6.19: Axial Displacement of the Middle Node for the Global Lateral Buckle Case

Figure 6.19 above show that the global buckle case is quite complex, there is no evident trend in the two cases. Table 6.5 below show the walk per cycle for each of the cases.

Radius [m]	Curve Length [m]	Walk per Cycle [m]
250	50	0.0279
	100	0.0587
	150	0.0693
	200	0.1419
400	50	0.0255
	100	0.0416
	150	0.0985
	200	0.2291

Table 6.5: Seabed Slope Values for the Detailed Case

The table above show that the walk per cycle for each lateral buckle case is larger than the walk per cycle for the base case. This imply that this case do not confirm the theory presented in Section 3.3.4 regarding buckle feed-in, and that the walk per cycle in fact increase when a lateral buckle occur. For a given radius, the walk per cycle generally increase for increasing curve lengths. How much the walk per cycle increase, seem to depend on the radius of the curve.

Figure 6.20 and Figure 6.21 below show the effective axial friction force for the r =250 [m], c = 200 [m] case and the r =400 [m], c = 200 [m] case.

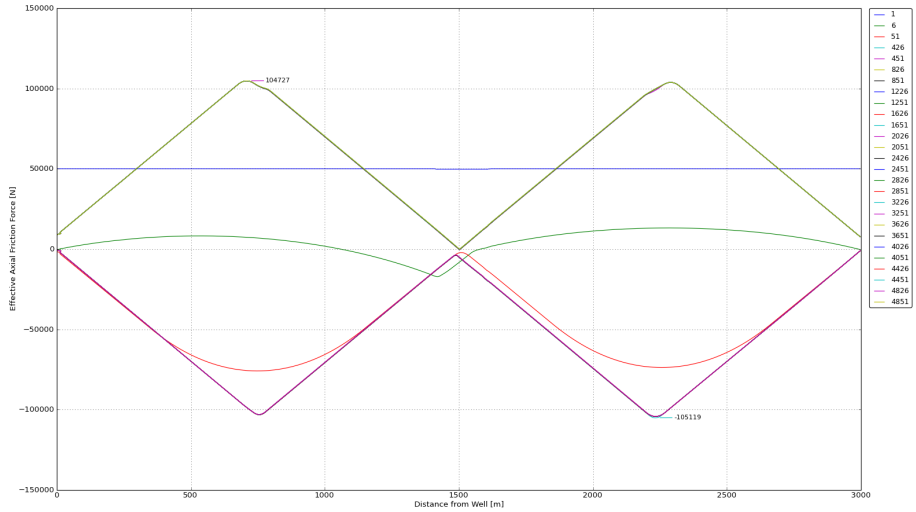

Figure 6.20: Effective Axial Friction Force for r =250 [m] and c = 200 [m]

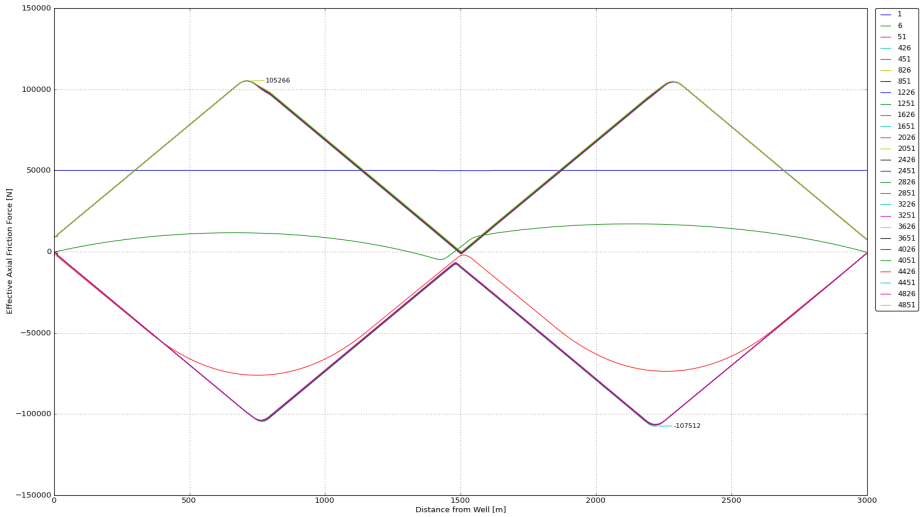

Figure 6.21: Effective Axial Friction Force for r =400 [m] and c = 200 [m]

Although the walk per cycle for the r =400 [m], c = 200 [m] case is much larger than

the walk per cycle for the r =250 [m], c = 200 [m] case, their effective axial friction force diagrams have the same shape and almost the same maximum compression and tensile forces. The diagrams above do resemble the diagram of a cyclically constrained pipeline. However, this do not match the pipeline's behaviour when observing it in Xpost, nor when considering the relatively large walk per cycle the pipelines in the two cases experience.

The pipelines are allowed to move laterally in the buckle. This means that the pipelines are able to release the axial friction force by laterally buckle, and this behaviour is observed in Xpost. This imply that at the middle of the pipelines, the effective axial friction force is close to zero due to the possibility for further laterally buckle. The diagrams above show that this happens both at warm-up and cool-down.

6.6 Tension Created by a Steel Catenary Riser

In the last part of the sensitivity study the effect of a steel catenary riser attached to the cold end of the pipeline was assessed. The results from this case can be seen in Figure 6.22 and Table 6.6 below.

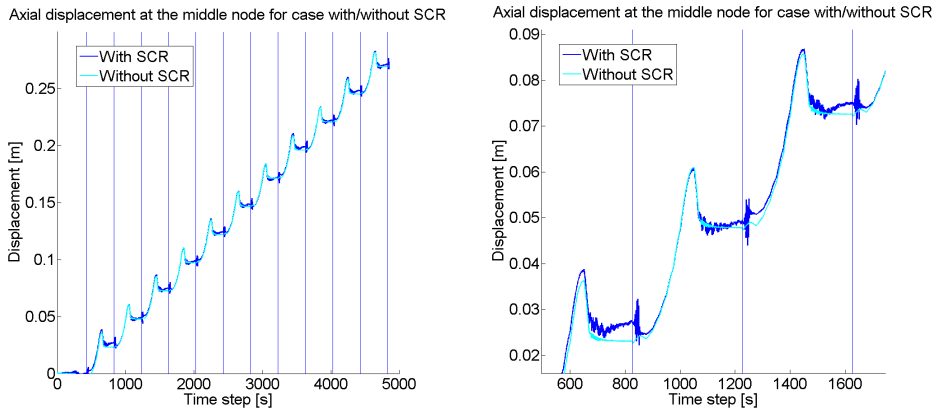

(a) Displacement for all Twelve Cycles

(b) Detailed View of the Displacement for two of the Cycles

Figure 6.22: Axial Displacement of the Middle Node with or without SCR

SCR Tension [N]	Walk per Cycle [m]	Walk per Cycle [mm]
5 000	0.0245	24.5
0	0.0246	24.6

Table 6.6: Walk per Cycle for the SCR Case

The figure and table above show that the permanent walk per cycle do not change much when applying a SCR load of 5 000 [N]. However, the nature of the axial movement change, as can be seen in Figure 6.22b. Here it is also apparent that the walk per cycle in the second heat-up cycle is a pinch higher for the "with SCR" case than for the "without SCR" case, but this stabilises in the subsequent cycles.

Figure 6.23 below show the effective axial friction force for this case.

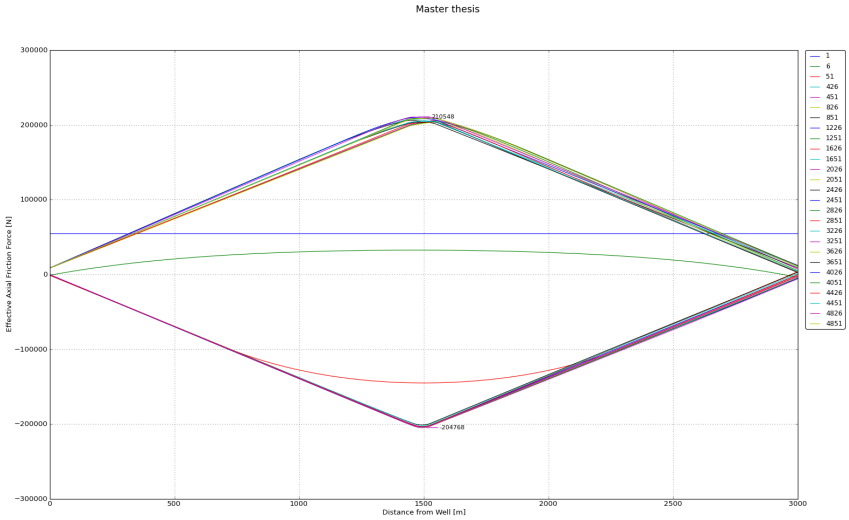

Figure 6.23: Effective Axial Friction Force for the SCR Case

The effective axial friction force diagram above is quite similar to the diagram of the base case, although there are some disturbances in the diagram. These disturbances can probably be traced back to the disturbances in Figure 6.22b above.

6.6.1 Analytical Results

The results from the seabed slope case were compared to analytical results, by using equations presented in the literature. These can be found in Section 5.2.7 in

the previous chapter.

The walk per cycle for both the numerical and analytical solution is presented in Figure 6.24 below.

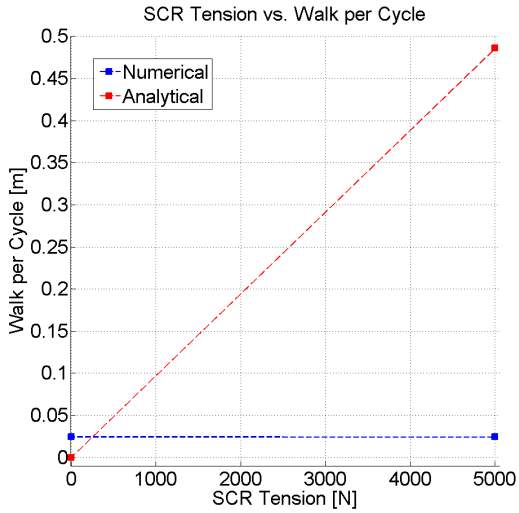

Figure 6.24: Axial Displacement of the Middle Node for the Numerical and Analytical Solutions

The difference between the results from the numerical and analytical analyses are quite large. As for the seabed slope case, the analytical result is zero walk per cycle for the base case, while the SIMLA model also includes temperature transients and thus add a walking inducing factor. When the SCR tension is added, the difference between the analytical and the numerical result is very large. There is no evident reason as to why there is such a large difference between the two solutions. The deviation seem to be too large to be explained by the theory of a conservative analytical model. There may be some assumptions and input values that are wrongly included in the analytical model in this case study. A further examination may be done in further work.

Chapter 7

Conclusion

In this thesis an introduction to offshore pipeline technology have been given, with a focus on topics relevant for pipeline walking. The behaviour of pipeline walking have been described, and its' mechanisms have been outlined together with a definition of the phenomenon. Several factors may have an impact on the walking behaviour. These have been presented, and later assessed through a sensitivity analysis.

When studying the seabed condition case it was found that the walk per cycle increase for increasing equivalent friction factor up to a value of $\mu_a = 1.1$, before the walk per cycle decrease as the equivalent friction factor continue to increase. For $\mu_a < 1.1$ the pipeline was found to be fully mobilised, with an increasing rate of walk per cycle. For very small μ_a the pipeline is fully mobilised before the transients have had the time to pass along the pipeline, and the walking thus stops at an early stage. For $\mu_a > 1.1$ the pipeline was found to be cyclically constrained, and increasing towards fully constrained behaviour as μ_a increased.

For the sloping seabed case is was found that the relationship between the seabed slope angle α and walk per cycle is approximately linear. For a seabed slope steeper than α = -0.55, the effect of a seabed slope will be larger than the effect of thermal transients along the pipeline. Consequently, the pipeline will move axially towards its' hot end. This is considered as the turning point for a pipeline resting on a sloping seabed. The lowest rate of walk per cycle was found for this turning point case, and it was found to be 1.2 [mm].

When introducing a global lateral buckle in the pipeline model, the walking behaviour changes. It was found that the peak displacement and elastic recovery distance increase, while the permanent walk per cycle is relatively quite small in comparison. However, the walk per cycle for the lateral buckle case is found to be much larger than the walk per cycle for the base case. The largest walk per cycle was found for the case with a curve radius of 400 [m] and curve length of 200 [m],

i.e. the case with the largest radius and curve length assessed in this part of the sensitivity study.

There was only time to test one case with a SCR attached to the cold end of the pipeline. The walk per cycle increased with 0.1 [mm] when introducing a SCR tension of 5 000 [N]. In addition the SCR tension gave fluctuations in the walking movement, which resulted in disturbances in the effective axial friction force diagram.

The comparison of the numerical results from SIMLA and the analytical results showed larger differences than expected. It is not immediately clear why the differences are so large, but the analytical model may be more conservative than the numerical one. In addition, the temperature transients are included inn all cases for the numerical model, which is not the case for the analytical one. This explains the deviation between the numerical base case and the analytical base case.

Chapter 8

Further Work

In this chapter further work, based on the findings in this thesis, is suggested. These recommendations are linked to the results from the sensitivity analysis, and the aim of these proposals are thus to better this sensitivity analysis for further studies.

To obtain a better understanding of the seabed conditions, the mobilisation length could be included as a separate sub-case. This way the results presented in [Tørnes et al., 2000] could be assessed. Another way of expanding the understanding of the pipe/soil interaction is to include a peak friction model for the equivalent axial friction factor. As a result, the understanding of a clay bottom's interaction with the pipeline could have been increased.

Only one SCR case have been presented due to time restrictions. For this reason it is natural to propose to conduct several SCR cases, with an increasing SCR tension for each sub-case.

As stated in Chapter 7, the accordance between the numerical and analytical results was not as good as envisioned. For further work with this sensitivity study, an analytical model more suited for comparison with the SIMLA model could be developed.

Lastly, one could expand the sensitivity study by combining the different walking inducing factors. This way it would be possible to see how the factors affect each other, and if some of them possibly counteract one another.

Bibliography

[IKM, 20xx] (20xx). Confedential IKM Report.

[Atkins et al., 2013] Atkins, ABS, Allseas, BP, BSEE, Bureau Veritas, Chevron, ConocoPhillips, DNV, ExxonMobil, Fugro, Inpex, JFE, Petrobras, Saipem, Shell, Statoil, Technip, Subsea7, Tonaris, Total, and Woodside (2013). The SAFEBUCK JIP. `www.safebuck.com`.

[Bai and Bai, 2005] Bai, Y. and Bai, Q. (2005). *Subsea Pipelines and Risers*. Elsevier Ltd.

[Brunner et al., 2006] Brunner, M. S., Qi, X., Zheng, J., and Chao, J. (2006). Combined Effect of Flowline Walking and Riser Dynamic Loads on HP/HT Flowline Design. *The Offshore Technology Conference 2006*.

[Bruton and Carr, 2011] Bruton, D. and Carr, M. (2011). Overview of the SAFEBUCK JIP. *The Offshore Technology Conference 2011*.

[Bruton et al., 2005] Bruton, D., Carr, M., Crawford, M., and Poiate, E. (2005). The Safe Design on Hot On-Bottom Pipelines with Lateral Buckling using the Design Guideline Developed by the SAFEBUCK Joint Industry Project. *The Deep Offshore Technology Conference 2005*.

[Bruton et al., 2008] Bruton, D., Carr, M., White, D. J., and Cheuk, J. C. Y. (2008). Pipe-Soil Interaction During Lateral Buckling and Pipeline Walking - The SAFEBUCK JIP.

[Carr et al., 2008] Carr, M., Sinclair, F., and Bruton, D. (2008). Pipeline Walking - Understanding the Field Layout Challenges and Analytical Solutions Developed for the SAFEBUCK JIP. *Society of Petroleum Engineers*, September:1–9.

[Foss, 2013] Foss, P. (2013). Guidance, Spring of 2013.

[Guo et al., 2005] Guo, B., Song, S., Chacko, J., and Ghalambor, A. (2005). *Offshore Pipelines*. Elsevier Inc.

[Jee, 2013] Jee (2013). Course Material for The Subsea Pipeline Design Course held for employees at IKM Ocean Design in Trondheim, March 2013.

[MARINTEK, 2013] MARINTEK (2013). Sintef. `http://www.sintef.no/home/MARINTEK/Software/Oil-and-Gas/`.

[MATLAB, 2013] MATLAB (2013). MATLAB. `www.mathworks.se/products/matlab/`.

[Perinet and Simon, 2011] Perinet, D. and Simon, J. (2011). Lateral Buckling and Pipeline Walking Mitigation in Deep Water. *The Offshore Technology Conference 2011*.

[Sævik, 2013] Sævik, S. (2013). Guidance, Spring of 2013.

[Sævik et al., 2012] Sævik, S., Økland, O. D., Baarholm, G. S., and Gjøsteen, J. K. Ø. (2012). SIMLA Version 3.15.11 User Manual.

[Tørnes et al., 2000] Tørnes, K., Ose, B. A., Jury, J., and Thomson, P. (2000). Axial Creeping of High Temperature Flowlines caused by Soil Ratcheting. *Proceedings of ETCE/OMAE2000 Joint Conference Energy for the New Millenium*.

Appendix A

The Effective Axial Friction Force for All Cases

This appendix includes all plots showing the effective axial friction forces for all cases in the sensitivity study.

A.1 The Seabed Conditions

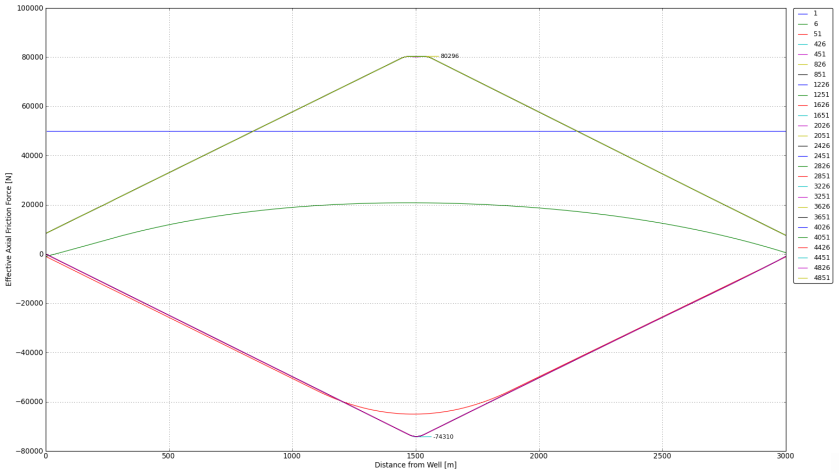

Figure A.1: The Effective Axial Friction Force for $\mu = 0.10$

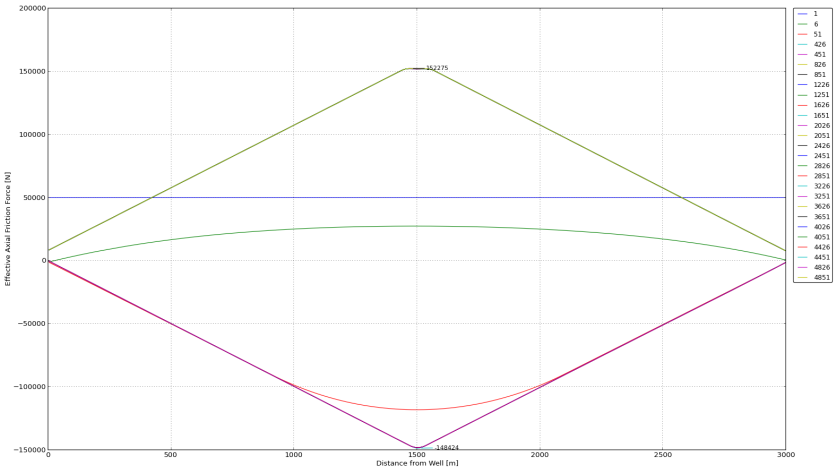

Figure A.2: The Effective Axial Friction Force for $\mu = 0.20$

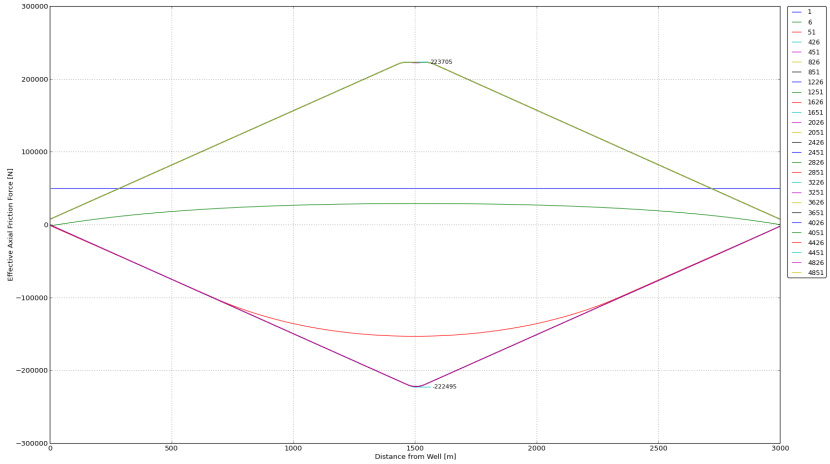

Figure A.3: The Effective Axial Friction Force for $\mu = 0.30$

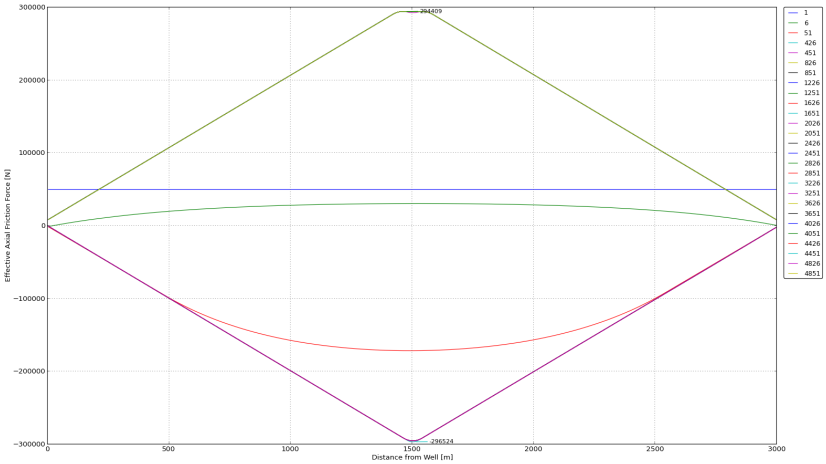

Figure A.4: The Effective Axial Friction Force for $\mu = 0.40$

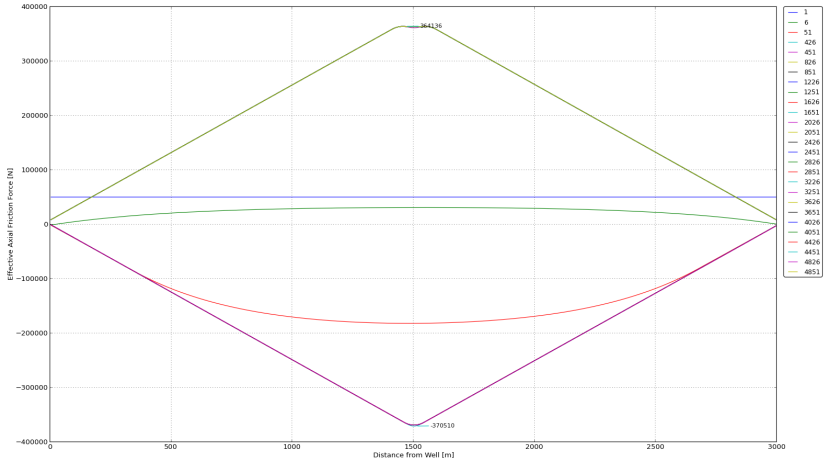

Figure A.5: The Effective Axial Friction Force for $\mu = 0.50$

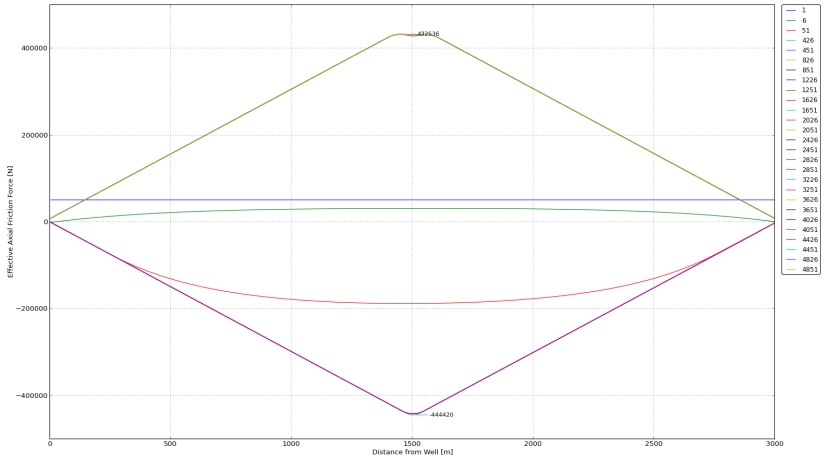

Figure A.6: The Effective Axial Friction Force for $\mu = 0.60$

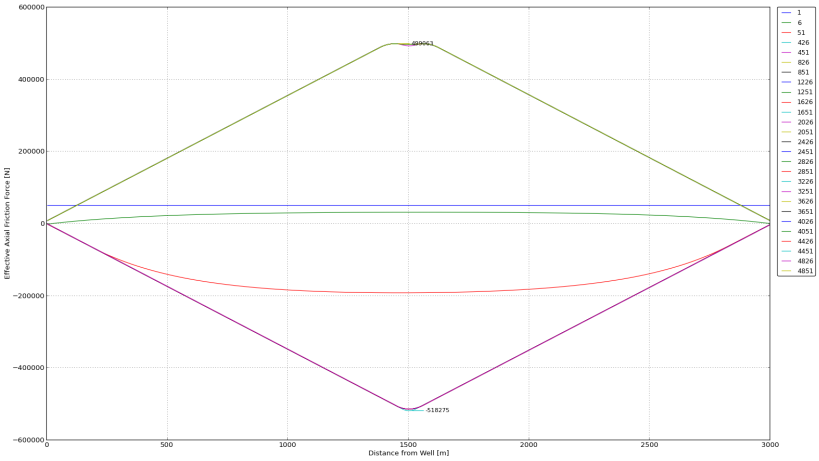

Figure A.7: The Effective Axial Friction Force for $\mu = 0.70$

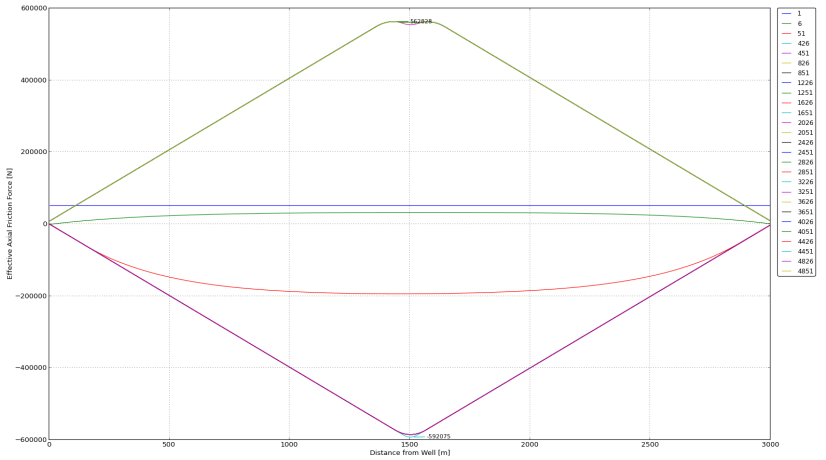

Figure A.8: The Effective Axial Friction Force for $\mu = 0.80$

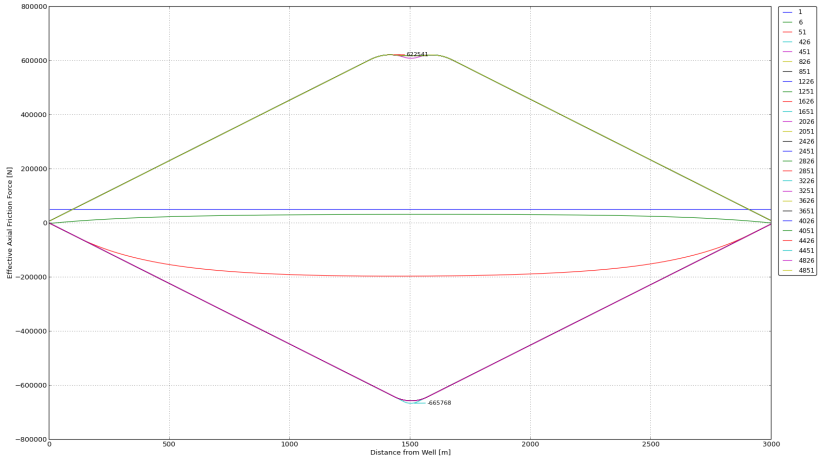

Figure A.9: The Effective Axial Friction Force for $\mu = 0.90$

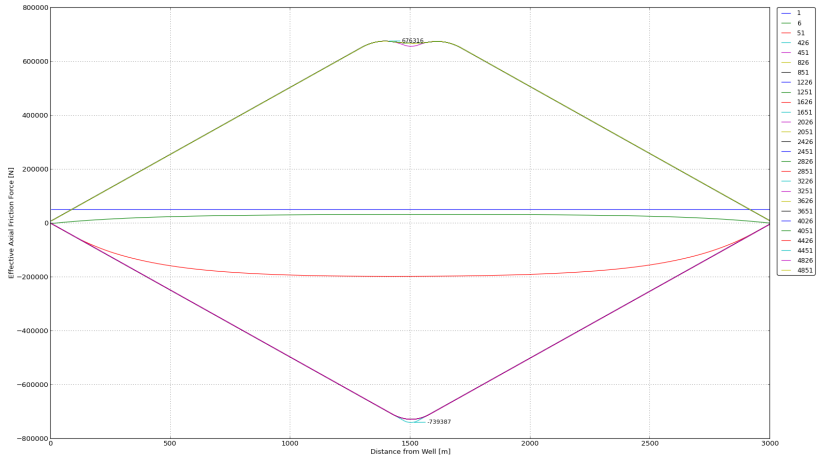

Figure A.10: The Effective Axial Friction Force for $\mu = 1.00$

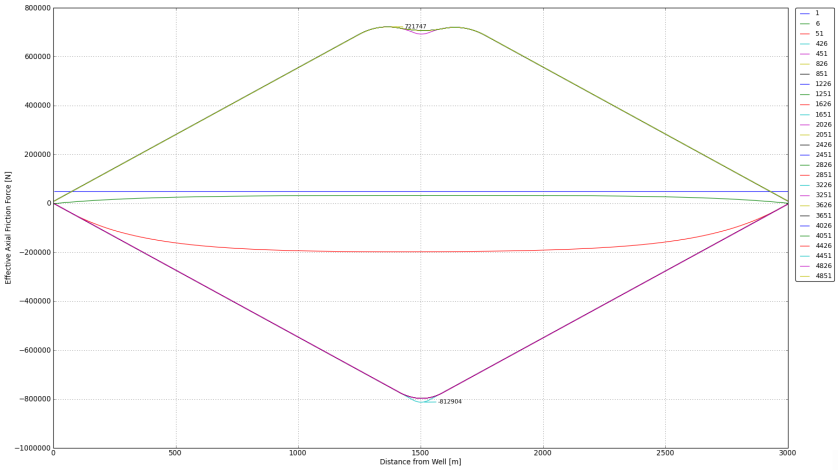

Figure A.11: The Effective Axial Friction Force for $\mu = 1.10$

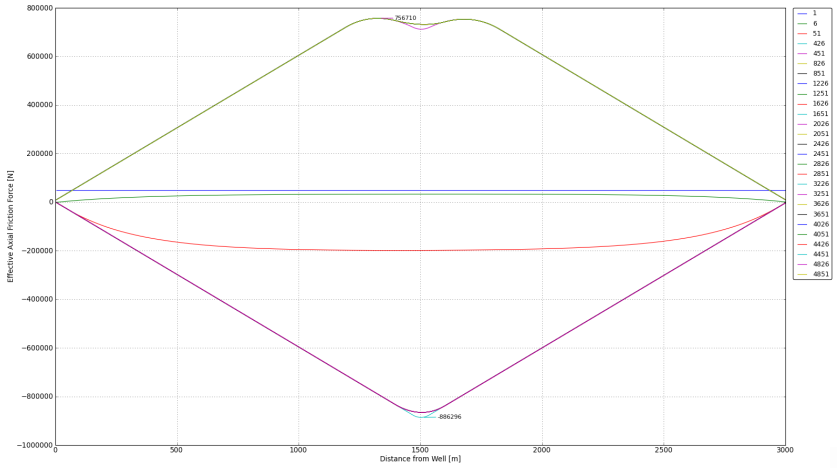

Figure A.12: The Effective Axial Friction Force for $\mu = 1.20$

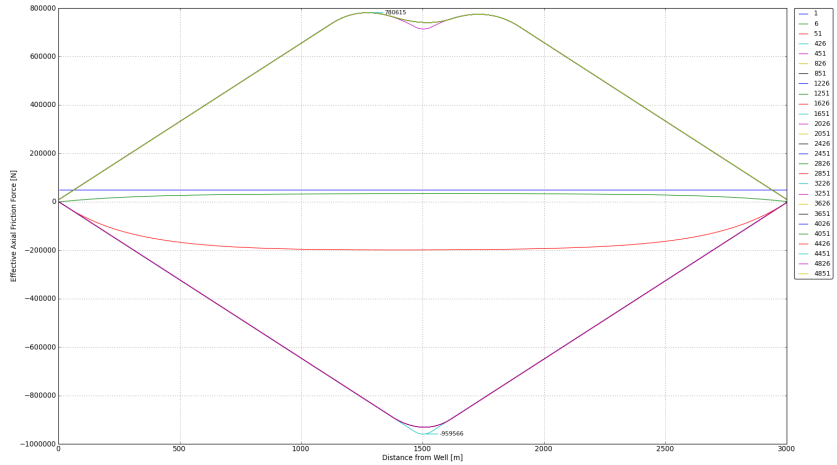

Figure A.13: The Effective Axial Friction Force for $\mu = 1.30$

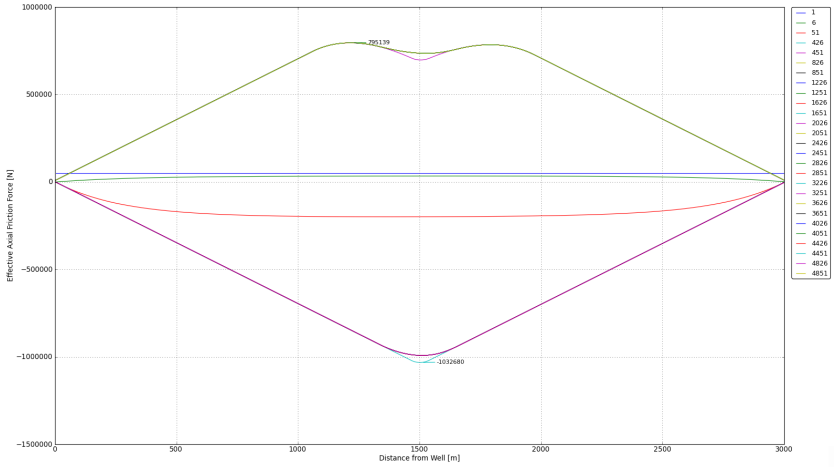

Figure A.14: The Effective Axial Friction Force for $\mu = 1.40$

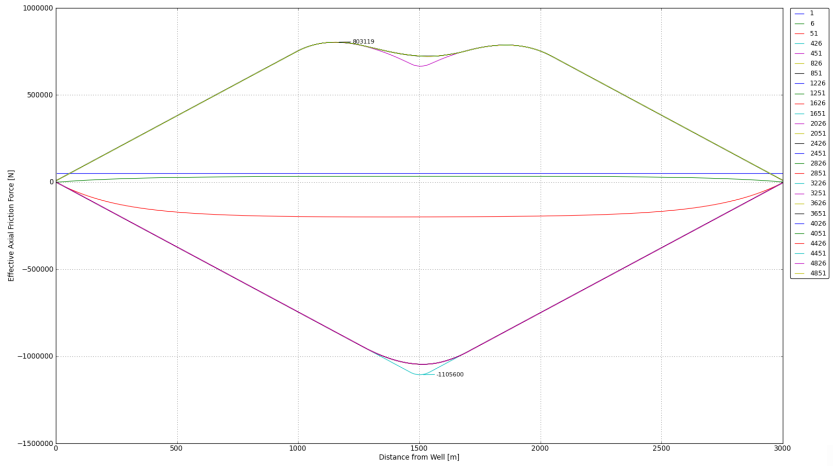

Figure A.15: The Effective Axial Friction Force for $\mu = 1.50$

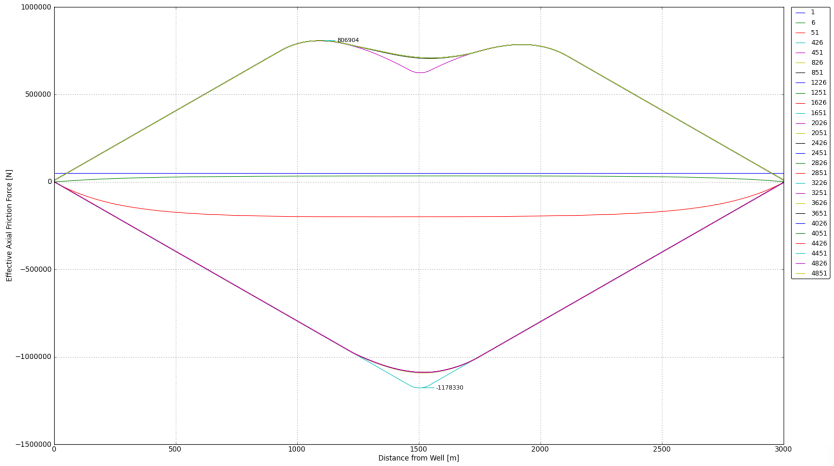

Figure A.16: The Effective Axial Friction Force for $\mu = 1.60$

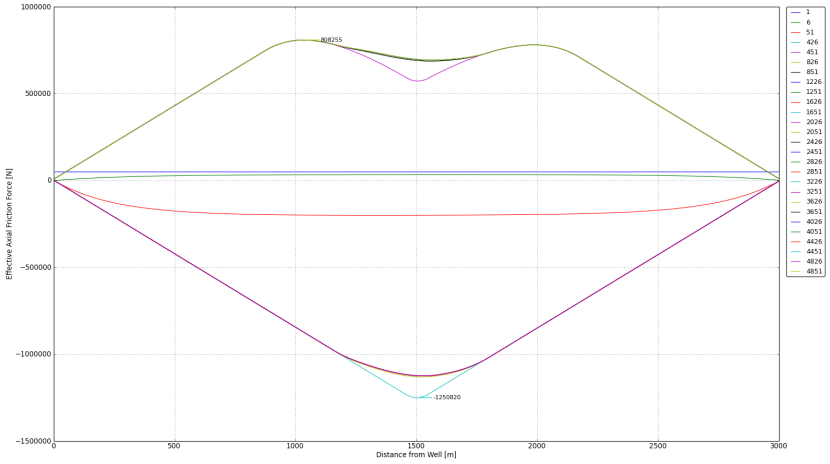

Figure A.17: The Effective Axial Friction Force for $\mu = 1.70$

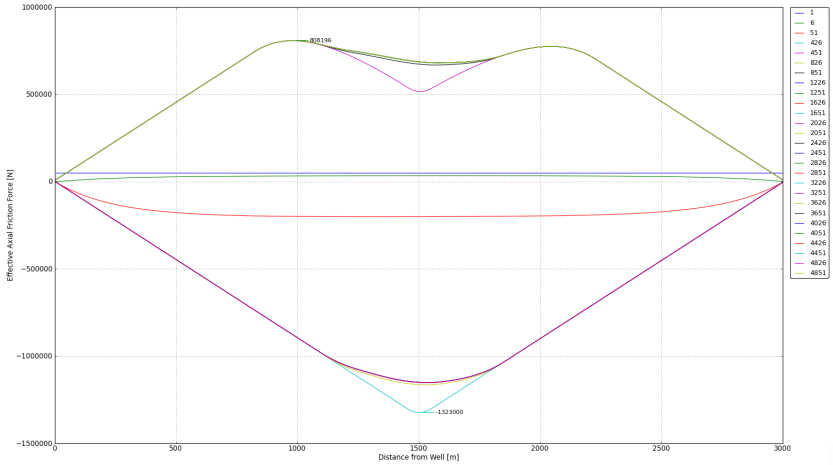

Figure A.18: The Effective Axial Friction Force for $\mu = 1.80$

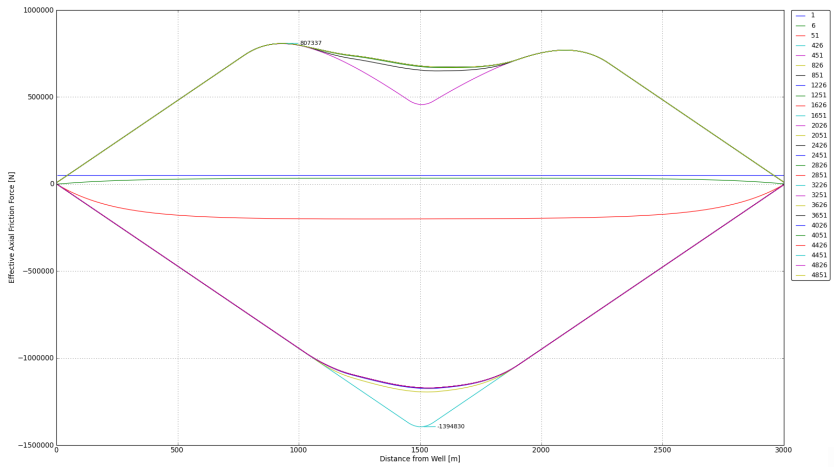

Figure A.19: The Effective Axial Friction Force for $\mu = 1.90$

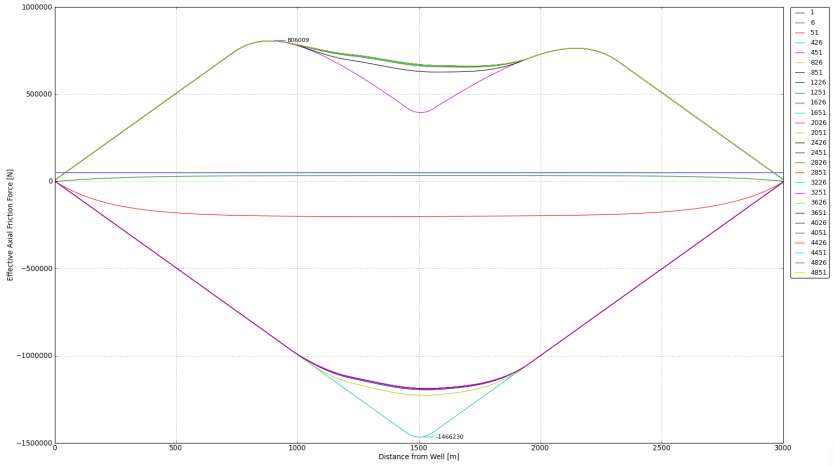

Figure A.20: The Effective Axial Friction Force for $\mu = 2.00$

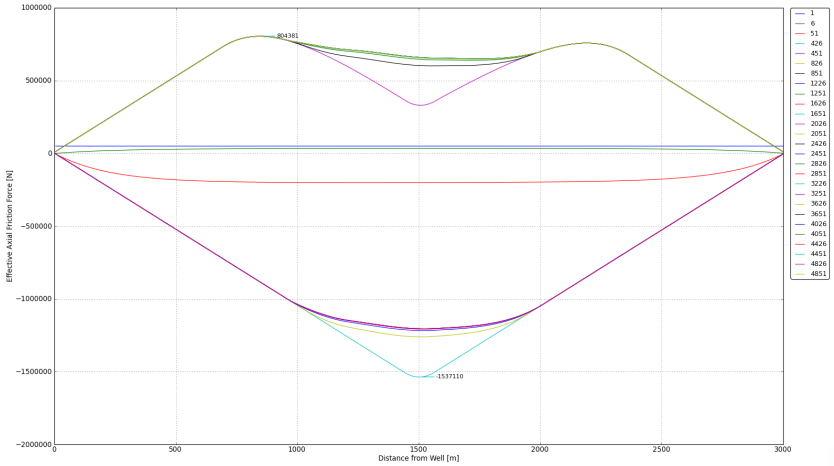

Figure A.21: The Effective Axial Friction Force for $\mu = 2.10$

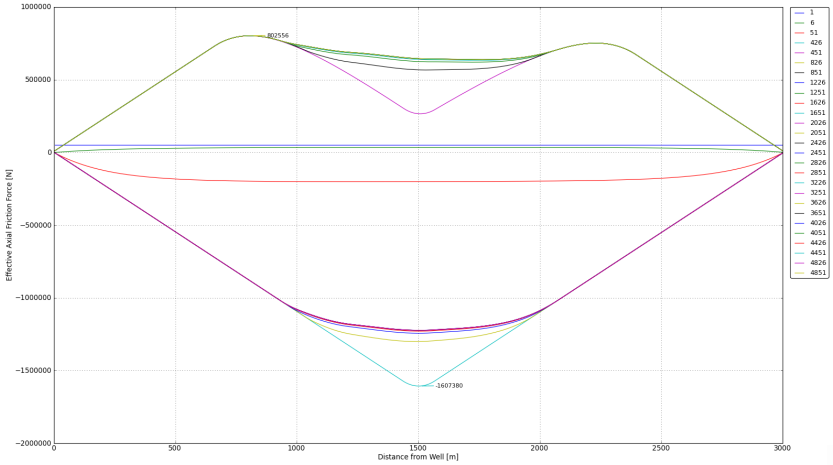

Figure A.22: The Effective Axial Friction Force for $\mu = 2.20$

A.2 The Seabed Slope

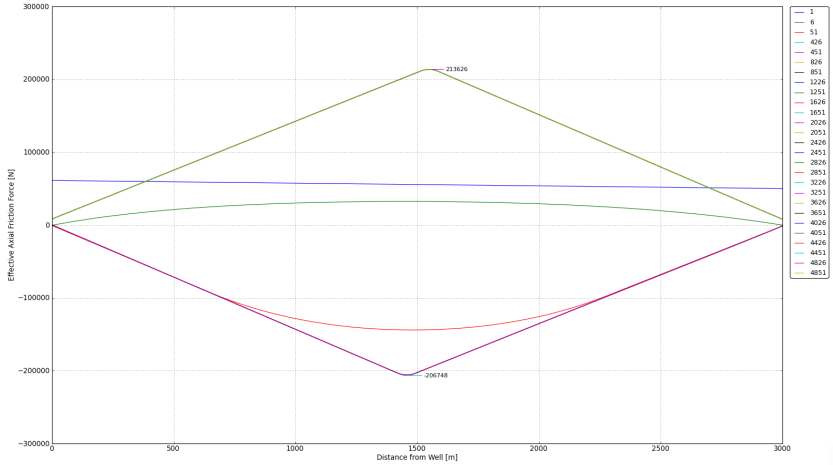

Figure A.23: The Effective Axial Friction Force for $\alpha = 0.5$

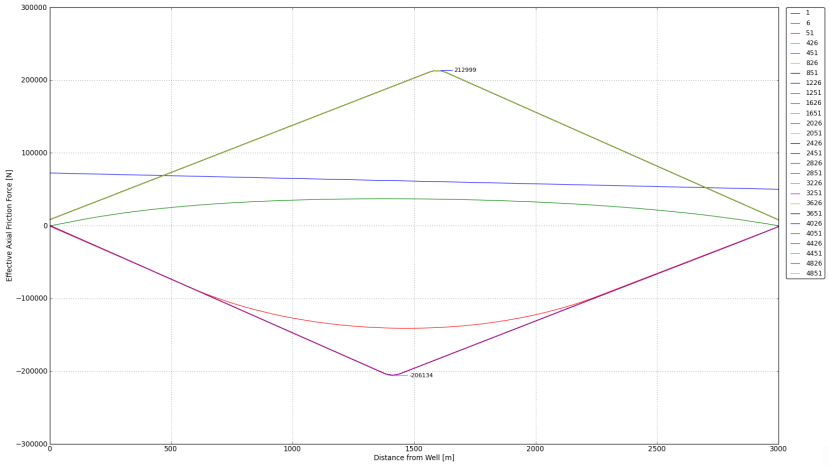

Figure A.24: The Effective Axial Friction Force for $\alpha = 1.0$

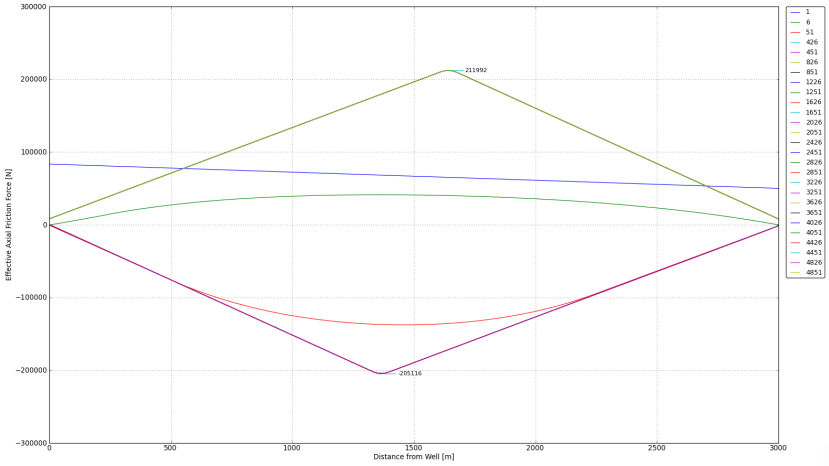

Figure A.25: The Effective Axial Friction Force for $\alpha = 1.5$

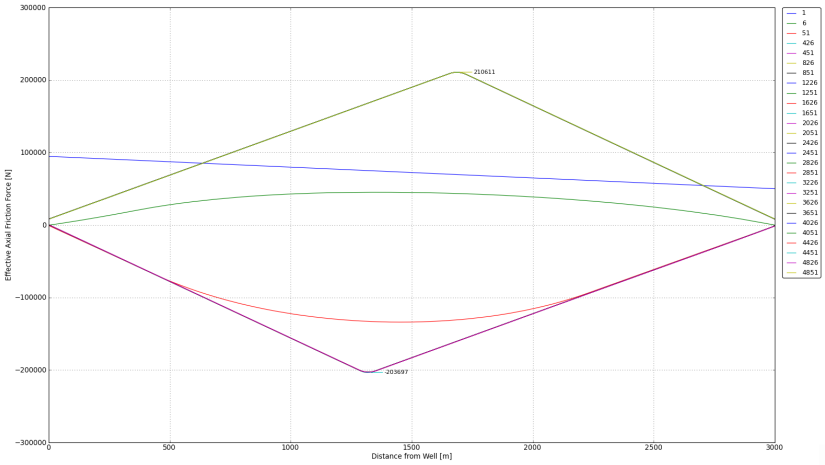

Figure A.26: The Effective Axial Friction Force for $\alpha = 2.0$

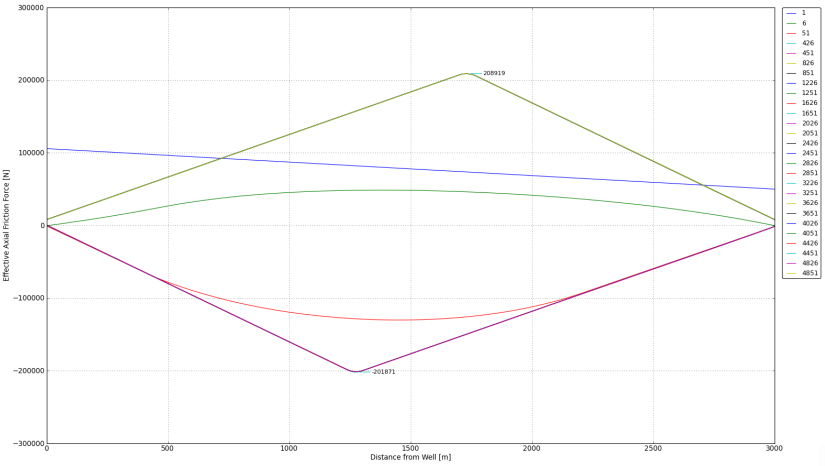

Figure A.27: The Effective Axial Friction Force for $\alpha = 2.5$

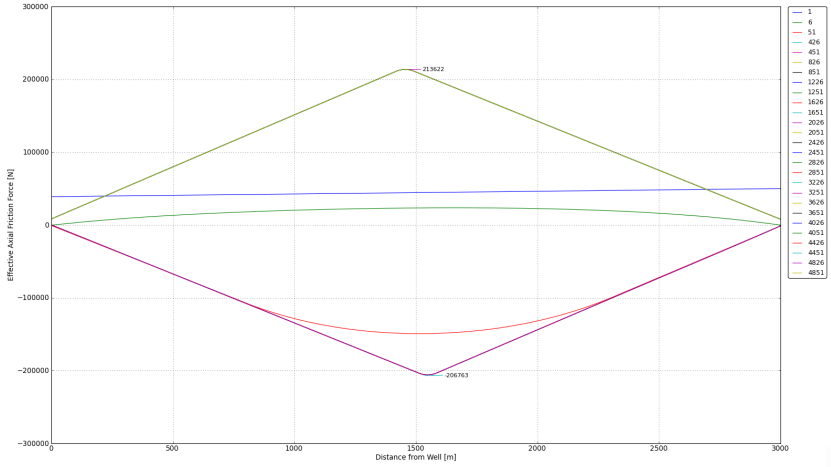

Figure A.28: The Effective Axial Friction Force for α = -0.5

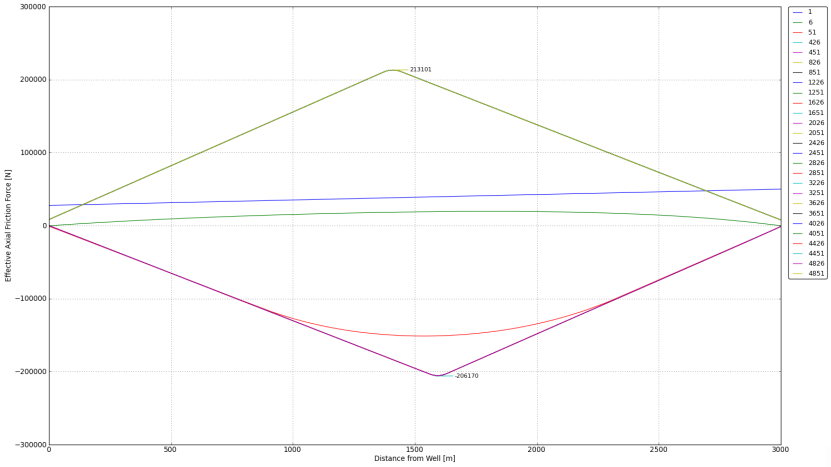

Figure A.29: The Effective Axial Friction Force for α = -1.0

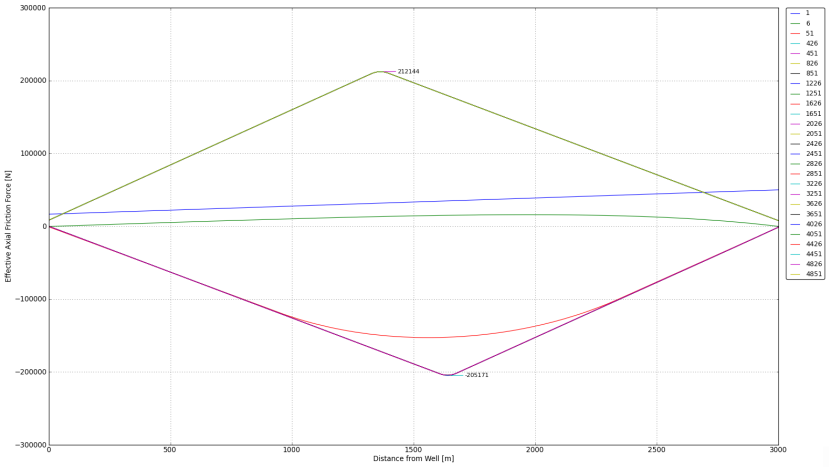

Figure A.30: The Effective Axial Friction Force for α = -1.5

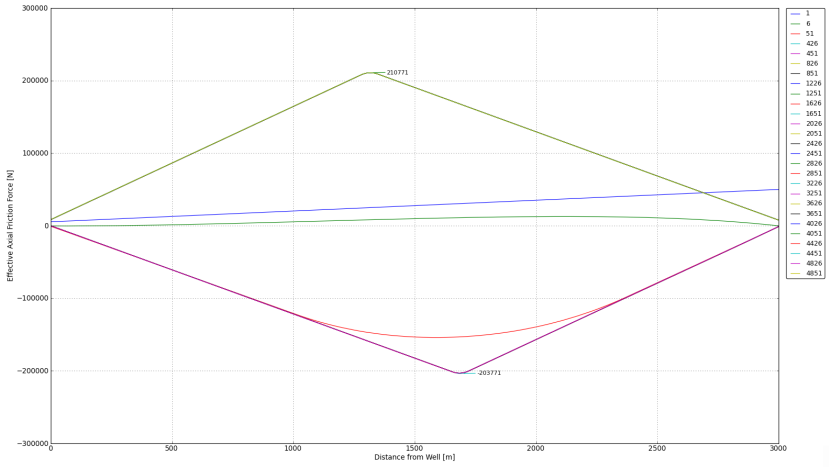

Figure A.31: The Effective Axial Friction Force for α = -2.0

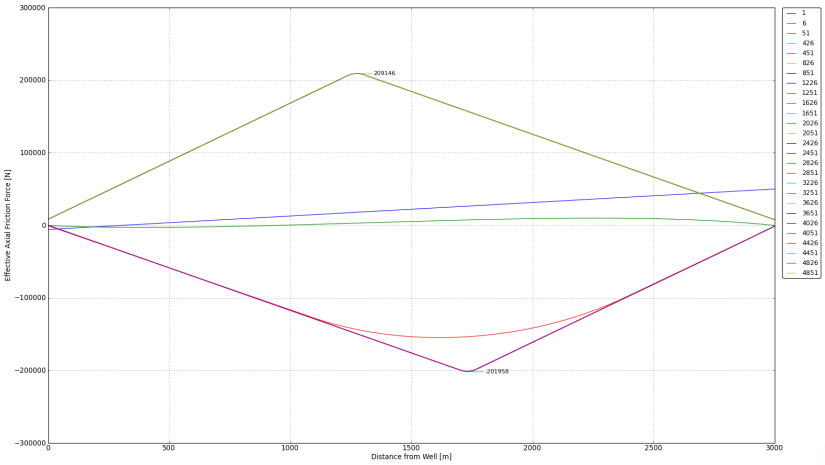

Figure A.32: The Effective Axial Friction Force for α = -2.5

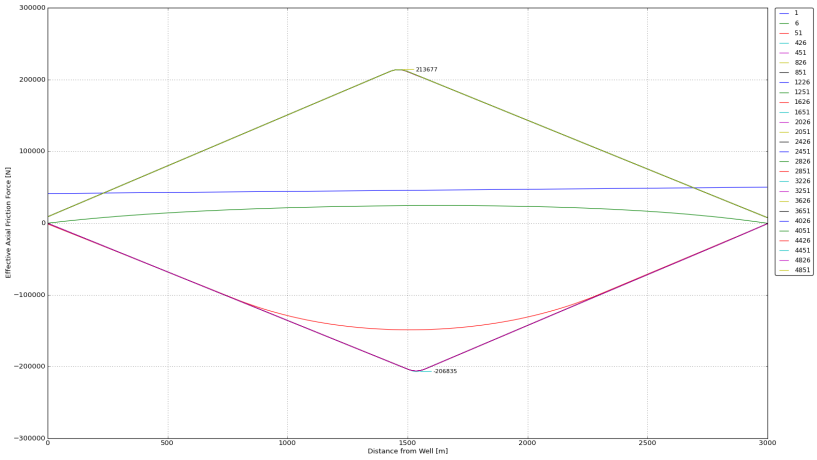

Figure A.33: The Effective Axial Friction Force for α = -0.40

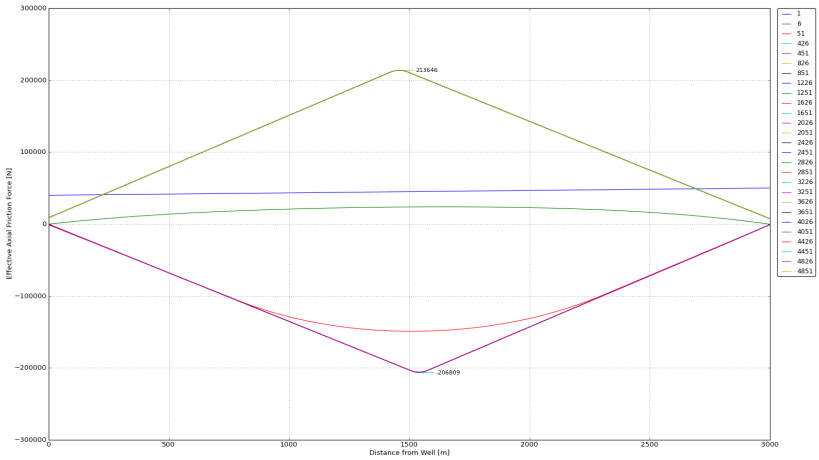

Figure A.34: The Effective Axial Friction Force for α = -0.45

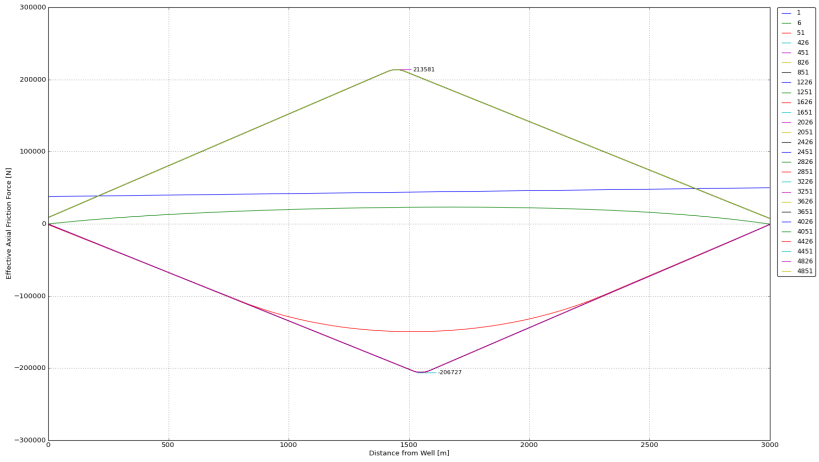

Figure A.35: The Effective Axial Friction Force for α = -0.55

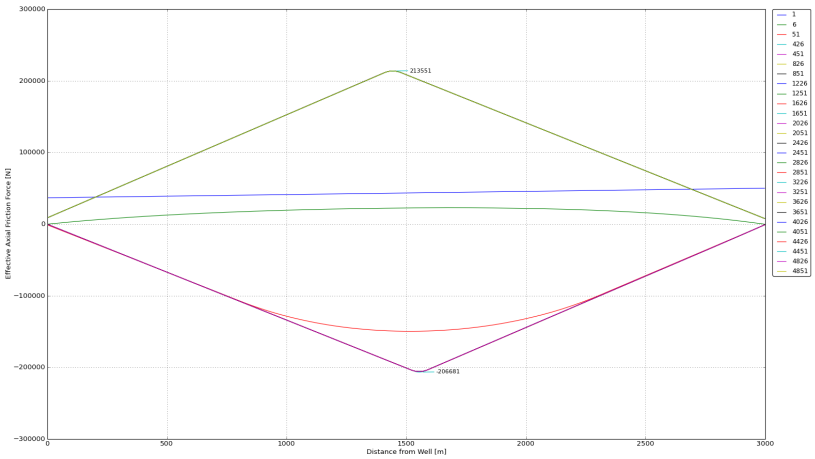

Figure A.36: The Effective Axial Friction Force for α = -0.60

A.3 Pipeline with Global Lateral Buckle

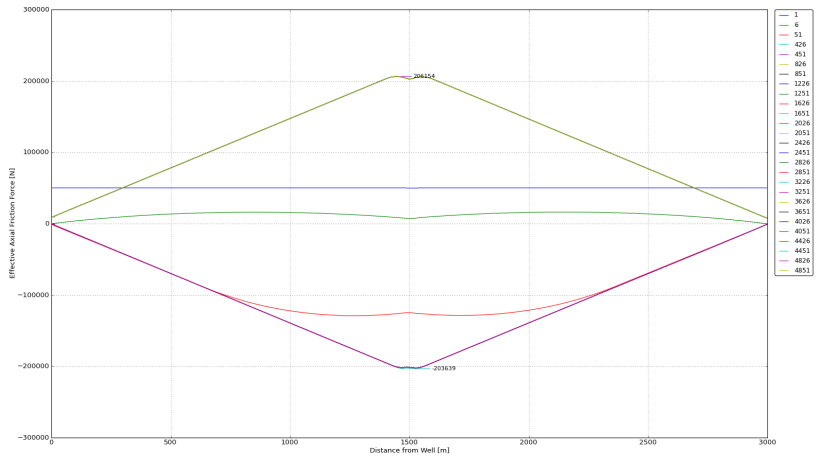

Figure A.37: The Effective Axial Friction Force for Radius of 250 [m] and a Curve Length of 50 [m]

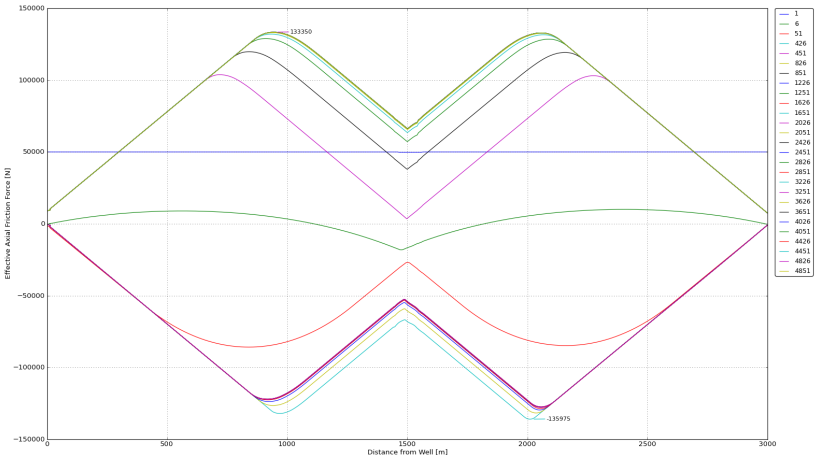

Figure A.38: The Effective Axial Friction Force for Radius of 250 [m] and a Curve Length of 100 [m]

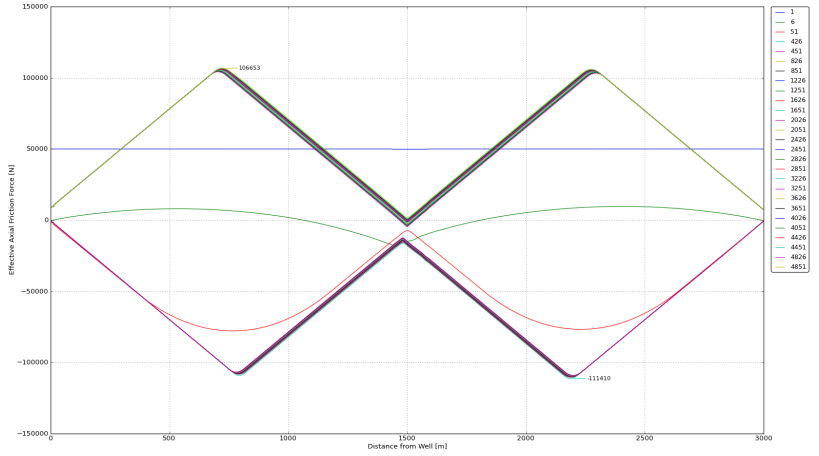

Figure A.39: The Effective Axial Friction Force for Radius of 250 [m] and a Curve Length of 150 [m]

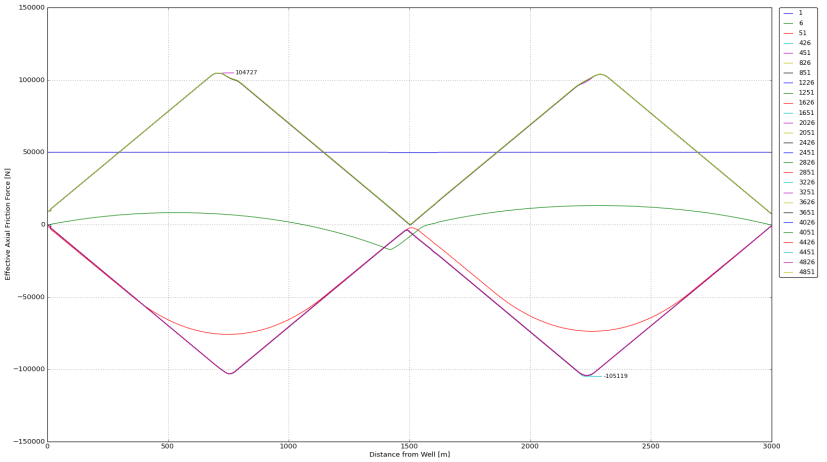

Figure A.40: The Effective Axial Friction Force for Radius of 250 [m] and a Curve Length of 200 [m]

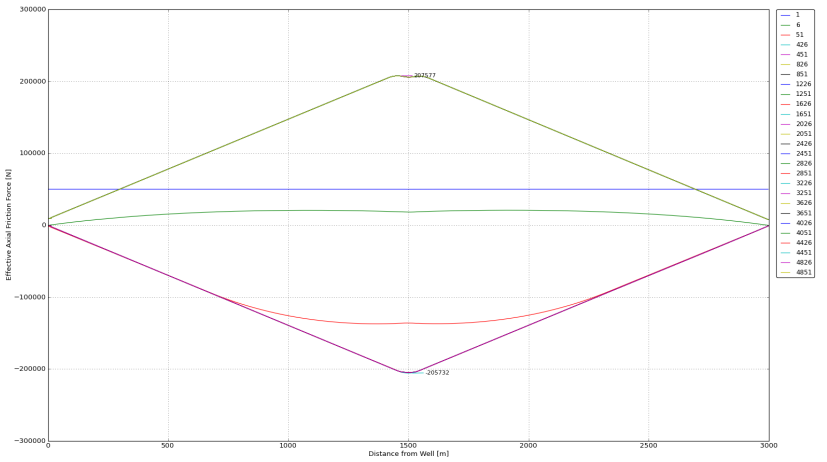

Figure A.41: The Effective Axial Friction Force for Radius of 400 [m] and a Curve Length of 50 [m]

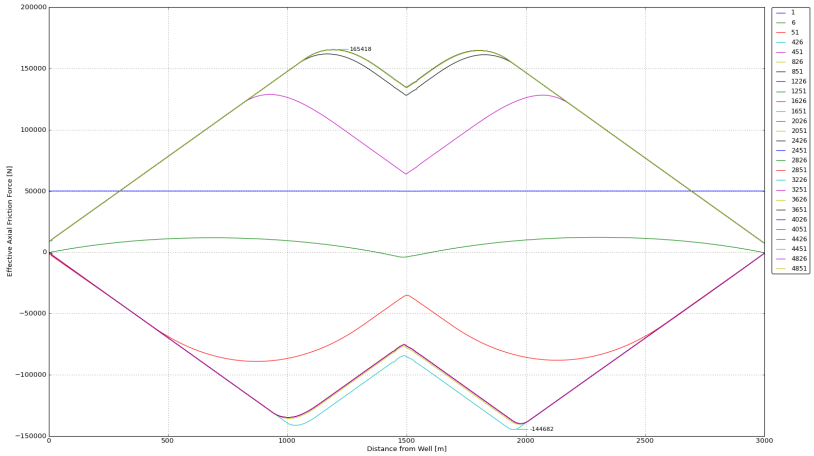

Figure A.42: The Effective Axial Friction Force for Radius of 400 [m] and a Curve Length of 100 [m]

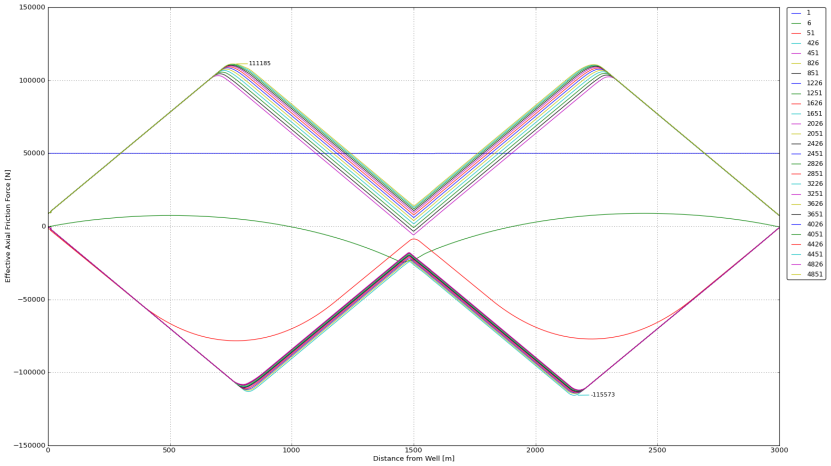

Figure A.43: The Effective Axial Friction Force for Radius of 400 [m] and a Curve Length of 150 [m]

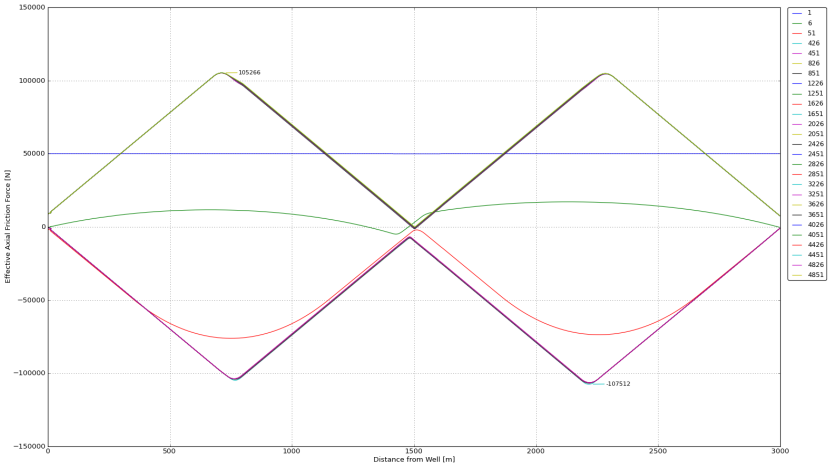

Figure A.44: The Effective Axial Friction Force for Radius of 400 [m] and a Curve Length of 200 [m]

A.4 Tension Created by a Steel Catenary Riser

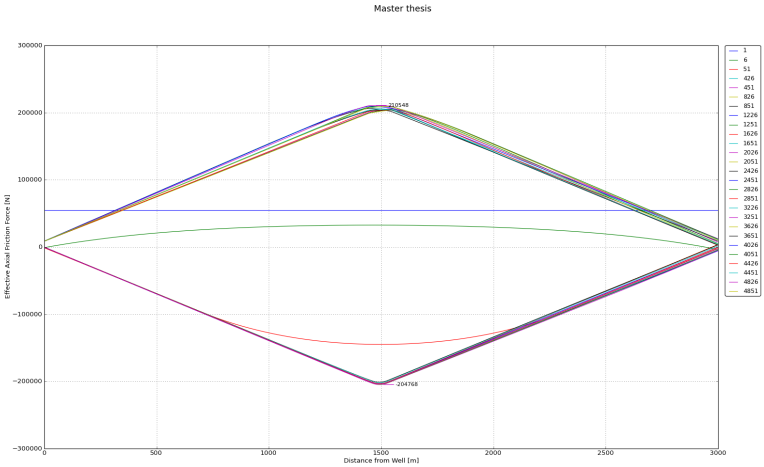

Figure A.45: The Effective Axial Friction Force for the SCR Case

Appendix B

Results from MATLAB

This appendix includes all results printed to screen by MATLAB for all cases in the sensitivity study.

B.1 The Seabed Conditions

```
Walk per cycle for
..equivalent friction factor = 0.10 [-] is 0.0088 [m]
..equivalent friction factor = 0.20 [-] is 0.0169 [m]
..equivalent friction factor = 0.30 [-] is 0.0267 [m]
..equivalent friction factor = 0.40 [-] is 0.0359 [m]
..equivalent friction factor = 0.50 [-] is 0.0434 [m]
..equivalent friction factor = 0.60 [-] is 0.0498 [m]
..equivalent friction factor = 0.70 [-] is 0.0558 [m]
..equivalent friction factor = 0.80 [-] is 0.0612 [m]
..equivalent friction factor = 0.90 [-] is 0.0655 [m]
..equivalent friction factor = 1.00 [-] is 0.0682 [m]
..equivalent friction factor = 1.10 [-] is 0.0694 [m]
..equivalent friction factor = 1.20 [-] is 0.0692 [m]
..equivalent friction factor = 1.30 [-] is 0.0673 [m]
..equivalent friction factor = 1.40 [-] is 0.0640 [m]
..equivalent friction factor = 1.50 [-] is 0.0594 [m]
..equivalent friction factor = 1.60 [-] is 0.0541 [m]
..equivalent friction factor = 1.70 [-] is 0.0482 [m]
..equivalent friction factor = 1.80 [-] is 0.0422 [m]
..equivalent friction factor = 1.90 [-] is 0.0307 [m]
..equivalent friction factor = 2.00 [-] is 0.0254 [m]
..equivalent friction factor = 2.10 [-] is 0.0206 [m]
..equivalent friction factor = 2.20 [-] is 0.0163 [m]
```

Figure B.1: The Walk per Cycle for the Seabed Conditions Cases

```
The overall walk after 12 cycles
..for the middle node with equivalent friction factor = 0.10
is 0.0965 [m]
..for the middle node with equivalent friction factor = 0.20
is 0.1859 [m]
..for the middle node with equivalent friction factor = 0.30
is 0.2929 [m]
..for the middle node with equivalent friction factor = 0.40
is 0.3945 [m]
..for the middle node with equivalent friction factor = 0.50
is 0.4764 [m]
..for the middle node with equivalent friction factor = 0.60
is 0.5472 [m]
..for the middle node with equivalent friction factor = 0.70
is 0.6130 [m]
..for the middle node with equivalent friction factor = 0.80
is 0.6726 [m]
..for the middle node with equivalent friction factor = 0.90
is 0.7192 [m]
..for the middle node with equivalent friction factor = 1.0
is 0.7489 [m]
..for the middle node with equivalent friction factor = 1.10
is 0.7620 [m]
..for the middle node with equivalent friction factor = 1.20
is 0.7593 [m]
..for the middle node with equivalent friction factor = 1.30
is 0.7386 [m]
..for the middle node with equivalent friction factor = 1.40
is 0.7019 [m]
..for the middle node with equivalent friction factor = 1.50
is 0.6514 [m]
..for the middle node with equivalent friction factor = 1.60
is 0.5927 [m]
..for the middle node with equivalent friction factor = 1.70
is 0.5285 [m]
..for the middle node with equivalent friction factor = 1.80
is 0.4623 [m]
..for the middle node with equivalent friction factor = 2.0
is 0.3361 [m]
..for the middle node with equivalent friction factor = 2.10
is 0.2773 [m]
..for the middle node with equivalent friction factor = 2.20
is 0.2261 [m]
```

Figure B.2: The Overall Walk for the Seabed Conditions Cases

B.2 The Seabed Slope

```
The overall walk after 12 cycles is 0.2712 [m] for the middle node
The overall walk after 12 cycles is 0.5452 [m] for the middle node
The overall walk after 12 cycles is 0.9597 [m] for the middle node
The overall walk after 12 cycles is 1.3885 [m] for the middle node
The overall walk after 12 cycles is 1.8071 [m] for the middle node
The overall walk after 12 cycles is 2.2320 [m] for the middle node

Walk per cycle for 0.0 [degreees] is 0.0247 [m]
Walk per cycle for 0.5 [degreees] is 0.0472 [m]
Walk per cycle for 1.0 [degreees] is 0.0813 [m]
Walk per cycle for 1.5 [degreees] is 0.1168 [m]
Walk per cycle for 2.0 [degreees] is 0.1513 [m]
Walk per cycle for 2.5 [degreees] is 0.1865 [m]


The overall walk after 12 cycles is 0.2712 [m] for the middle node
The overall walk after 12 cycles is -0.0039 [m] for the middle node
The overall walk after 12 cycles is -0.4181 [m] for the middle node
The overall walk after 12 cycles is -0.8492 [m] for the middle node
The overall walk after 12 cycles is -1.2732 [m] for the middle node
The overall walk after 12 cycles is -1.7052 [m] for the middle node

Walk per cycle for 0.0 [degreees] is 0.0247 [m]
Walk per cycle for -0.5 [degreees] is 0.0021 [m]
Walk per cycle for -1.0 [degreees] is -0.0320 [m]
Walk per cycle for -1.5 [degreees] is -0.0676 [m]
Walk per cycle for -2.0 [degreees] is -0.1025 [m]
Walk per cycle for -2.5 [degreees] is -0.1382 [m]
```

Figure B.3: The Walk per Cycle for the Seabed Slope Cases

```
The overall walk on seabed slope after 12 cycles
..is 0.0889244000 [m] for the middle node
..is 0.0430215000 [m] for the middle node
..is -0.0039183000 [m] for the middle node
..is -0.0442672000 [m] for the middle node
..is -0.0815202000 [m] for the middle node

Walk per cycle for seabed slope
..angle = -0.40 [degrees] is 0.0098910600 [m]
..angle = -0.45 [degrees] is 0.0059764900 [m]
..angle = -0.50 [degrees] is 0.0021001100 [m]
..angle = -0.55 [degrees] is -0.0011713600 [m]
..angle = -0.60 [degrees] is -0.0042076400 [m]
```

Figure B.4: The Walk per Cycle for the Detailed Seabed Slope Cases

B.3 Pipeline with Global Lateral Buckle

```
The walk per cycle for the r = 250 [m] case
 is 0.0279 [m] for a curve length of 50 [m]
 is 0.0587 [m] for a curve length of 100 [m]
 is 0.0693 [m] for a curve length of 150 [m]
 is 0.1419 [m] for a curve length of 200 [m]

The walk per cycle for the r = 400 [m] case
 is 0.0255 [m] for a curve length of 50 [m]
 is 0.0416 [m] for a curve length of 100 [m]
 is 0.0985 [m] for a curve length of 150 [m]
 is 0.2291 [m] for a curve length of 200 [m]
```

Figure B.5: The Walk per Cycle for the Global Lateral Buckle Case

B.4 Tension Created by a Steel Catenary Riser

```
The overall walk after 12 cycles for Case 1
is 0.2731 [m]
The overall walk after 12 cycles for Case 2
is 0.2705 [m]

The walk per cycle for case 1
 is 0.0245 [m]
The walk per cycle for case 2
 is 0.0246 [m]
```

Figure B.6: The Overall Walk and Walk per Cycle for the SCR Case